AEDC-TR-68-198

cy₁

EVALUATION OF WIND TUNNEL TESTS ON AFMDC MONORAIL CONE- AND SPIKE-NOSE SLED CONFIGURATIONS AT MACH NUMBERS FROM 2.0 TO 5.0

W. T. Strike, Jr., and E. J. Lucas

ARO, Inc.

December 1968

VON KÁRMÁN GAS DYNAMICS FACILITY
ARNOLD ENGINEERING DEVELOPMENT CENTER
AIR FORCE SYSTEMS COMMAND
ARNOLD AIR FORCE STATION, TENNESSEE

NOTICES

EVALUATION OF WIND TUNNEL TESTS
ON AFMDC MONORAIL CONE- AND SPIKE-NOSE SLED
CONFIGURATIONS AT MACH NUMBERS FROM 2.0 TO 5.0

W. T. Strike, Jr., and E. J. Lucas

ARO, Inc.

FOREWORD

The work reported herein was done at the request of the Air Force Missile Development Center (AFMDC), Air Force Systems Command (AFSC), under Program Element 6540215F, Project 6876.

The results presented were obtained by ARO, Inc. (a subsidiary of Sverdrup & Parcel and Associates, Inc.), contract operator of the Arnold Engineering Development Center (AEDC), AFSC, Arnold Air Force Station, Tennessee, under Contract F40600-69-C-0001. These tests were conducted during the period from February 27 to April 23, 1968, under ARO Project No. VA0795, and the manuscript was submitted for publication on August 12, 1968.

This technical report has been reviewed and is approved.

Eugene C. Fletcher
Lt Colonel, USAF
AF Representative, VKF
Directorate of Test

Roy R. Croy, Jr.
Colonel, USAF
Director of Test

ABSTRACT

An evaluation was made of the results of wind tunnel tests on
0.4-scale models of two Holloman Air Force Base monorail rocket-
sled configurations. The sled models consisted of a cylindrical body
with forward and aft splitter wedges and slippers and with an inter-
changeable 15-deg cone nose and spike nose. The wind tunnel tests
were conducted at Mach numbers 2, 3, 4, and 5 and over a Reynolds
number range (based on the sled body diameter) from 0.22 to 1.92
million. The sled model was sting supported over a scaled replica of
the Holloman track rail which was supported on a sharp-leading-edge
ground plane (flat plate). The test results consist of static force meas-
urements obtained from a six-component strain-gage balance. Also,
pitot pressure flow field surveys were made over the ground plane and
model rail in the region occupied by the sled model. The following
model parameters were varied during the test: the location of the sled
relative to the rail tip and also to the ground plane leading edge, the
height of the sled body above the rail surface, the gap between the
slipper and rail surface, and the sled roll angle. The results presented
include an evaluation of the influence of the sled slippers, the free-
stream Reynolds number, and the Mach number on the aerodynamic
loading of the sled.

CONTENTS

ILLUSTRATIONS

TABLES

APPENDIXES

NOMENCLATURE

A_i	Reference area, projected base area, in.^{2} (A_1, A_2, and A_3 equals 11.32, 12.22 and 13.46 in.^{2}, respectively)
$C_{A,b}$	Base drag coefficient, $(p_\infty - p_b)/q_\infty$.
$C_{A,F}$	Frictional drag coefficient, frictional drag/$(q_\infty A_i)$
$C_{A,T}$	Total drag coefficient, total axial force/$(q_\infty A_i)$
C_D	Forebody drag coefficient, $C_{A,T} - C_{A,b}$
C_ℓ, $C_{\ell,s}$	Rolling-moment coefficient about the balance and sled slipper reference point, respectively, rolling moment/$(q_\infty A_i d)$
C_m, $C_{m,s}$	Pitching-moment coefficient about balance and sled slipper reference point, respectively, pitching moment/$(q_\infty A_i \ell)$

C_N	Normal-force coefficient, $F_N/(q_\infty A_i)$
$C_{N,A}$	Aft slipper loading coefficient, $F_{N,A}/(q_\infty A_i)$
$C_{N,F}$	Forward slipper loading coefficient, $F_{N,F}/(q_\infty A_i)$
C_n, $C_{n,s}$	Yawing-moment coefficient about the balance and sled slipper reference point, respectively, yawing moment$/(q_\infty A_i \ell)$
C_Y	Side-force coefficient, $F_Y/(q_\infty A_i)$
C_ψ	Rolling-moment coefficient about the rail edge, rolling moment$/(q_\infty A_i d)$
d	Diameter of the cylindrical body, 3.60 in.
F_A	Forebody axial force, kips (10^3 lb$_f$)
$F_{A,T}$	Total axial force, lb$_f$
F_b	Base axial force, lb$_f$
F_N	Normal force, kips
$F_{N,A}$	Loading on the aft slipper or slipper support, kips (see Fig. 2)
$F_{N,F}$	Loading on the forward slipper or slipper support, kips (see Fig. 2)
$F_{R,k}$	Magnitude of a resultant force vector in the "k" plane, kips
F_Y	Side force, kips
h	Distance from the sled centerline to the rail surface, in.
h_g	Gap between slipper and the upper surface of the rail, in. (see Fig. I-1)
$h*$	Correlation parameter, $2\beta h/x_0$
ℓ	Reference length, distance between forward and aft slipper centerlines, 18.537 in.
ℓ_k	Normal distance between the forward slipper moment reference point and $F_{R,k}$ vector, in.
ℓ_s	Spike-nose length, 7.20 in.
M_L	Local Mach number based on p_p/p_∞
M_x, M_y, M_z	Rolling, pitching, and yawing moment about the balance axis in the wind tunnel coordinate system, in.-lb$_f$
M_∞	Free-stream Mach number

m	Tan θ (see Fig. 23)
p_b	Base pressure, psia
p_0'	Stagnation pressure downstream of a normal shock, psia
p_p	Probe pitot pressure, psia
p_∞	Free-stream static pressure, psia
q_∞	Free-stream dynamic pressure, psia
Re_d	Reynolds number based on model diameter of 3.6 in.
RT	Rail tip configuration (see Fig. 5)
u_∞	Free-stream or sled velocity, ft/sec
X, Y, Z	Right-hand coordinate system with X (+) upstream
X_R	Displacement of rail tip from ground plane leading edge, in.
X_S	Displacement of sled from ground plane leading edge, in.
x	Distance along ground plane, in.
x_k	Displacement of the "k" resultant force vector from moment reference point k = 1, 2, and 3 (see Appendix II), in.
x_n	Cone-nose length, 6.717 in.
x_o	Overall sled length, 31.02 in. for cone-nose sled and 31.50 in. for spike-nose sled
x_T	Axial transfer distance from balance reference to sled slipper reference point, 2.03 in.
α	Angle of attack, deg
β	$\sqrt{M_\infty^2 - 1}$
δ	Boundary-layer thickness, in.
δ_k	Angular orientation of the "k" resultant force vector (see Appendix II), deg
ϵ	Average grit size, in.
θ	Cone-nose half-angle, deg
μ_o	Mach angle, deg
ϕ	Roll angle, deg
ψ	Yaw angle, deg

SUBSCRIPTS

i   Variation in reference area to correspond to a change
                in the sled height (h)

k   Plane of the resultant force vector, k = 1, pitch axis
                plane; k = 2, yawing axis plane; and k = 3, roll axis
                plane (see Appendix II)

O, Q, R   Moment reference points defined in Appendix II

SECTION I
INTRODUCTION

The general purpose of this study is to determine if steady-state wind tunnel data can be used to adequately define the quasi-steady-state aerodynamic loading imposed on a full-scale, rocket-propelled, mono-rail sled vehicle. The quasi-steady-state forces on the sled refer to the mean values of the loadings on the sled as it accelerates and then coasts through the decelerating phase of its trajectory along the track. Superimposed on these full-scale, quasi-steady-state loadings are oscillatory forces produced, according to Ref. 1, by rail roughness, aerodynamic buffeting, and acoustics. The influence of these oscillatory forces on the sled are not included in the present analysis.

There are several basic differences between the flow over the full-scale vehicle as it moves along a track and the wind tunnel flow over a model used to simulate the sled structural environment. This full-scale track consists of one longitudinal section of a concrete channel supporting a steel rail. In the wind tunnel tests, a flat plate with a sharp leading edge and side plates is used to simulate the ground effects of this longitudinal section, and a scaled-down version of the rail is mounted on and extends upstream of the flat plate or ground plane leading edge.

In the wind tunnel, the sled bow wave interaction with the boundary layer on the ground and rail surfaces differs from the actual case. This difference could have a significant effect on the aerodynamic loading of the sled. Also, the rail and ground plane leading edges of the wind tunnel model may produce significant adverse local disturbances not present in the full-scale track tests, and, of course, the Reynolds number associated with the full-scale vehicle is much greater than that of the wind tunnel model. As a first step, therefore, the wind tunnel model configuration which best simulates the environment of the full-scale track vehicle must be selected and evaluated in terms of rail tip geometry and location, ground plane leading-edge location, and wind tunnel Reynolds number and Mach number. Thus, the wind tunnel test program included flow surveys to permit an evaluation of the flow field disturbance generated by the rail tip and ground plane leading edges and by the boundary-layer growth along the rail and ground plane. In the force phase of the test program, the influence of the rail tip geometry and its location relative to the sled position, the location of the sled relative to the ground plane leading edge, and the height of the sled above the rail on the sled loadings were investigated. In most cases, boundary-layer trips consisting of Carborundum® grit were used to maintain turbulent

1

flow over the model surface. Also, the influence of free-stream Mach number, slipper gap height, and sled roll angle were investigated.

The tests were conducted in the 40-in. supersonic tunnel (Gas Dynamic Wind Tunnel, Supersonic (A)) of the von Kármán Gas Dynamics Facility. The results were obtained at nominal Mach numbers of 2, 3, 4, and 5 at nominal Reynolds numbers (Re_d) from 0.22×10^6 to 1.92×10^6. The test data consisted of pitot pressure surveys of the region occupied by the sled model and measurement of the sled loads. A summary of the test parameters is listed in Table I. Schlieren, shadowgraph, oil flow, and vapor screen techniques were used as an aid in visually observing the local flow field patterns generated over the model.

SECTION II
DESCRIPTION OF THE EXPERIMENTAL EQUIPMENT

2.1 WIND TUNNEL

Tunnel A is a continuous, closed-circuit, variable density wind tunnel with an automatically driven flexible-plate nozzle and a 40- by 40-in. test section. The tunnel operates at Mach numbers from 1.5 to 6 at maximum stagnation pressures from 29 to 200 psia, respectively, and at stagnation temperatures up to 760°R (M_∞ = 6). Minimum operating pressures range from about one-tenth to one-twentieth of the maximum pressures.

2.2 MODEL AND BALANCE

The 0.40-scale model components consisted of the sled, internal balance, rail, and ground plane (flat plate with side plates) as shown in Fig. 1. The basic sled model had a cylindrical body with two interchangeable nose configurations consisting of a 15-deg cone and a 0.40-in.-diam spike (see Fig. 2), but did not have the pop-out air brakes proposed for use in the deceleration phase of the full-scale sled runs. The sled model which was supported by a balance and sting combination could be driven automatically through nominal distances of 2 in. vertically and 11.5 in. axially and rolled to any angle within a range of ±6 deg. Also, the rail had an axial travel of 8 in.

TABLE I

SUMMARY OF WIND TUNNEL TEST PARAMETERS

| Configuration	Free-Stream Mach Number, M_∞	(Reynolds Number/in.) x (3.6 in.) $Re_d \times 10^{-6}$	Sled Height, h, in.	Comments
(1) Cone Nose with Slippers Attached to the Sled	2.0, 3.0, 4.0, 5.0	Varied at each M_∞ range: 0.215 to 1.93	2.048	Model Run with Three Different Grit Sizes (40, 60, 80). Grit Applied to Model: 0.5-in. Band 1 in. from Cone and Spike Tip; 0.5-in. Band on Cylinder 1 in. from Shoulder; Strip on Splitter Wedge and Slipper Shoe.
	3.0	1.78	2.05	Varied Roll Angle from -2 to 3 deg.
	2.0, 3.0, 4.0, 5.0	Maximum at each M_∞ range: 1.52 to 1.93	2.048	Ran Various Rail and Sled Locations Relative to Leading Edge of Ground Plane. Range: X_S: -0.8 to 10.9 X_R: 17.63 to 25.63
(2) Spike Nose with Slippers Attached to Sled	2.0 and 3.0	Varied at each M_∞ range: 0.30 to 1.78		X_S 3.0 X_R 21.63
	4.0 and 5.0	0.66 to 1.93		X_R 25.63
(3) Spike Nose with Slippers Detached from Sled but in Same Position Attached to Rail	2.0 and 3.0	0.30 to 1.78		X_R 21.63
	4.0 and 5.0	0.66 to 1.93		X_R 25.63
(4) Cone Nose with Slippers Detached from Sled but in Same Position Attached to Rail	2.0 and 3.0	0.30 to 1.78		X_R 21.63 At M_∞ = 3.0 Removed Slippers from Rail and Varied Roll Angle from -1 to 4 deg
	4.0 and 5.0	0.66 to 1.93		X_R 25.63
(5) Same as (4)	3.0	0.21 to 1.78	2.448	X_R 21.63
(6) Cone Nose with Slippers Attached to Sled				
(7) Cone Nose with Slippers Detached from Sled but in Same Position Attached to Rail			3.00	
(8) Cone Nose with Slippers Attached to Sled				

a. Model Installed in Tunnel A
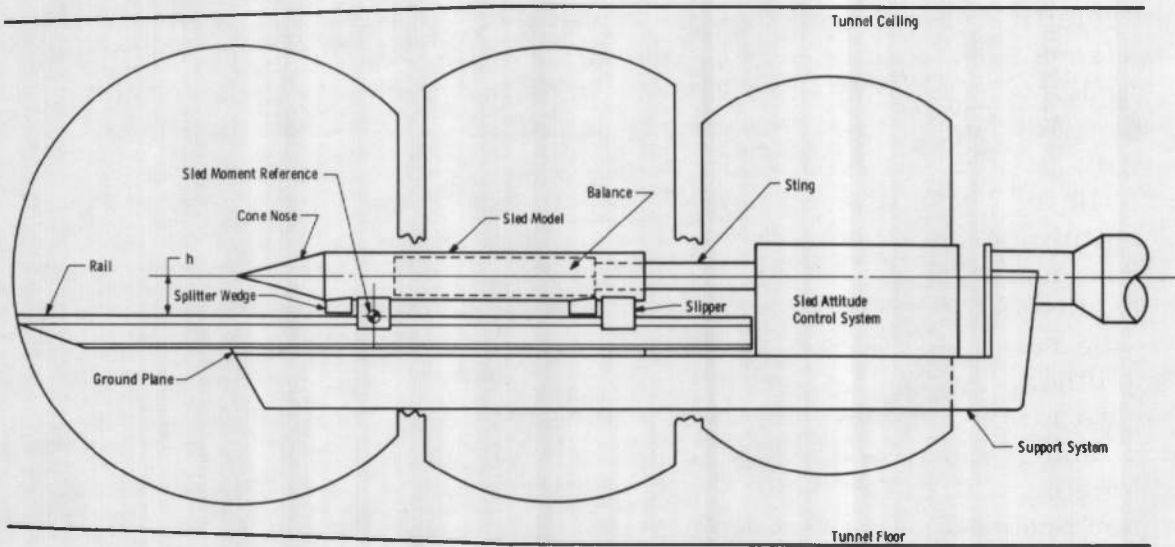
b. Model Nomenclature
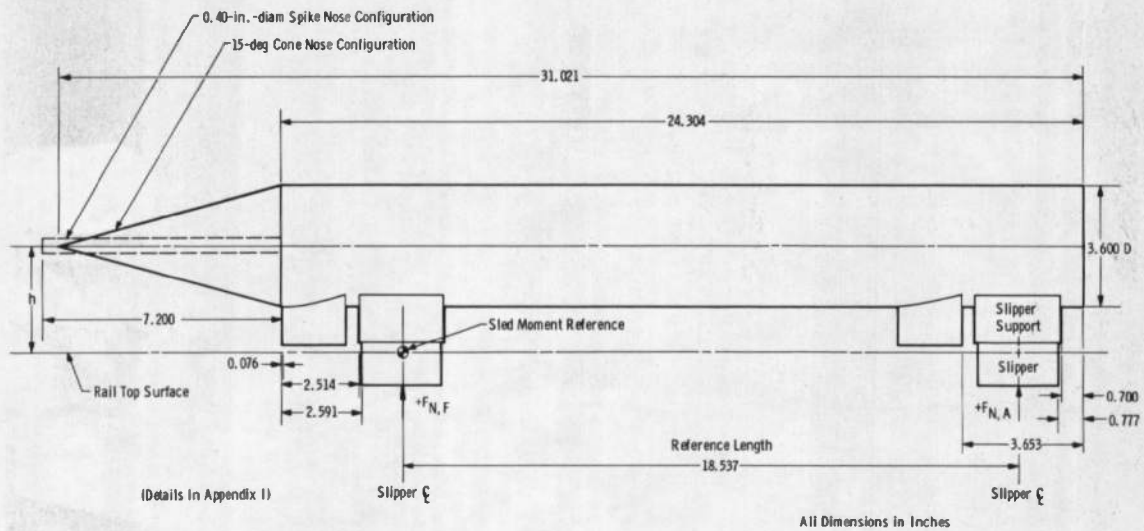Fig. 1 AFMDC Monorail Cone-Nose Sled Model

4

Fig. 2 Sled Configurations

A six-component strain-gage balance was used to measure the aerodynamic loading on the sled which was suspended over the model rail. The symmetrical gap between the rail and the sled slipper surfaces was approximately 0.125 in. (see Fig. I-1 in Appendix I). However, during these tests, the gap between the upper rail surface and slipper was reduced to 0.005 in. or less and, therefore, the lower extremities of the slipper were nearly 0.250 in. below the lower rail surfaces. When the gaps were being changed, fouling lights were used to indicate when contact existed between the model slippers and the rail. Additional model configuration details are given in Appendix I.

In the preliminary phase of the test program, a rake containing 60 pitot pressure probes (Fig. 3) was used to evaluate the flow field characteristics in the area occupied by the sled. These pitot pressure measurements provided an estimate of the boundary-layer thicknesses on the rail and ground plane and the strength of the compression waves and other disturbances generated by the rail and ground plane. As shown in Fig. 3b, the pressure probes located within 0.5 in. of the rail and ground plane surfaces (six at each survey location) had a diameter of 0.031 in. with a tube wall thickness of 0.004 in. The other probes located in the outer flow field region had a tube diameter of 0.065 in. with a wall thickness of 0.011 in.
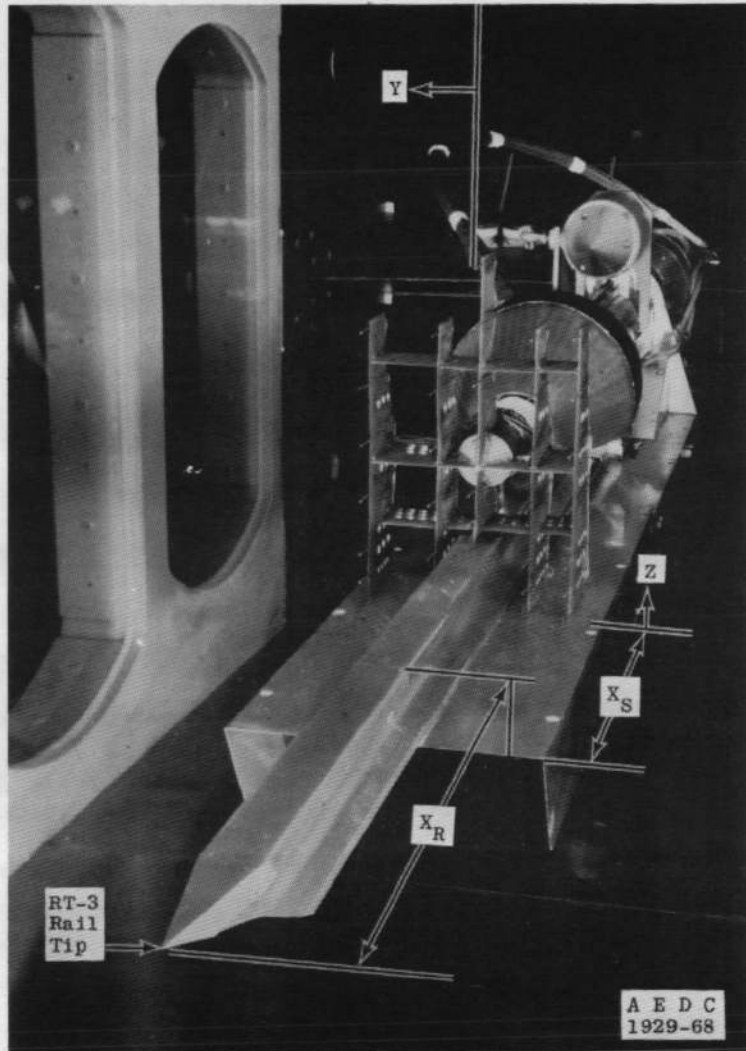
a. Flow Field Coordinates

b. Pitot Probe Details

Fig. 3 Flow Field Survey Probe Installed in Tunnel A

2.3 INSTRUMENTATION AND PRECISION OF RESULTS

The estimated uncertainties in the force and moment measurements, based on an analysis of the balance calibration results, are given below.

Component	Uncertainties	Repeatability of Data in Coefficient Form
Normal force, lbf	±0.15	±0.0022
Side force, lbf	±0.15	±0.0022
Axial force, lbf	±0.10	±0.0014
Pitching moment, in.-lbf	±0.50	±0.0004
Rolling moment, in.-lbf	±0.20	±0.0008
Yawing moment, in.-lbf	±0.15	±0.0001

(Based on M_∞ = 3.0 and q_∞ = 7.0 psia)

These uncertainties in the force measurements produced an estimated repeatability in the angular orientation of the resultant force vector (δ_1) of ±0.20 deg and the repeatability of the location of this resultant force vector (x_1) of ±0.6 percent of the characteristic model length (ℓ).

The model base pressures and rake pitot pressures were measured with 15-psid transducers. These transducers were calibrated for ranges of 1, 5, and 15 psia and have an estimated accuracy of 0.25 percent of the full-scale calibrated range used to record the pressure.

The location of the rail tip and sled relative to the ground plane leading edge was known to within 0.05 in.

SECTION III
RESULTS AND DISCUSSION

3.1 MODEL FLOW FIELD CHARACTERISTICS

Pitot pressure surveys were made over the ground plane and rail for the purpose of evaluating the uniformity of the flow in the region to be occupied by the sled model. These surveys were made only at Mach number 3.0 and at a Reynolds number (Re_d) of 1.8×10^6 for the three different rail tip configurations (see Fig. I-4).

A typical set of pitot pressure profiles in the area to be occupied by the sled is shown in Fig. 4. The Y coordinate represents the displacement of the pressure profile from the center of the rail. The probe

pressure (p_p) was normalized by the free-stream stagnation pressure downstream of a normal shock (p_O'). Therefore, for pressure ratios (p_p/p_O') of unity, the local and free-stream Mach numbers are identical. The nomenclature used in Fig. 4 to locate the survey probes and model rail tip is schematically shown in Fig. 3a.
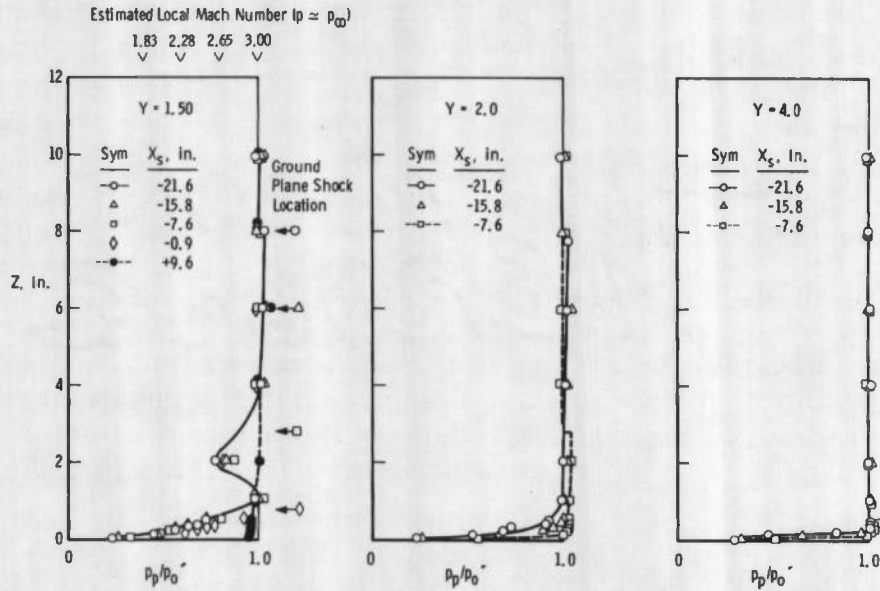
a. Fixed Rail Location (X_R = 21.6 in.), Variable Ground Plane Location
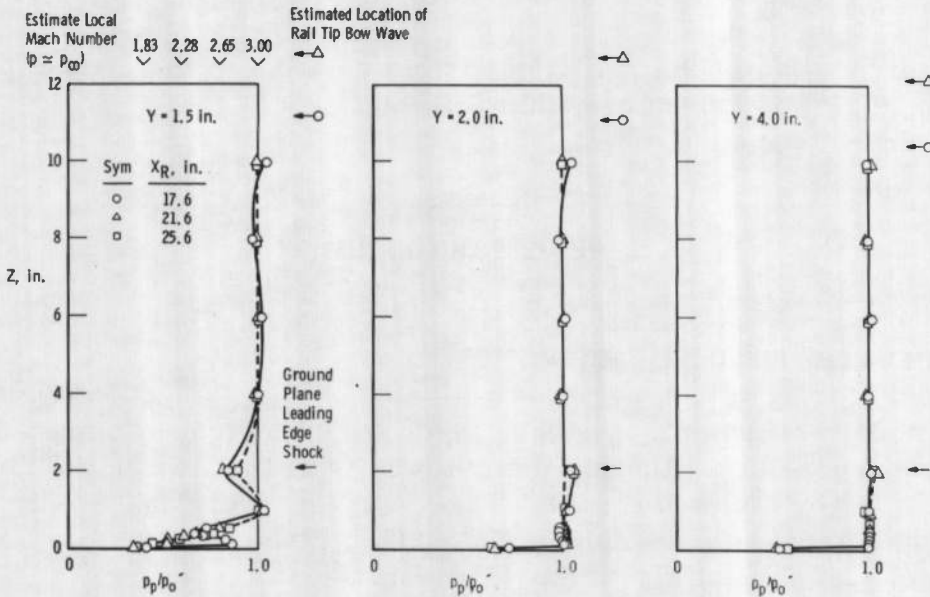
b. Fixed Ground Plane Location (X_S = −5.8 in.), Variable Rail Tip Location

Fig. 4 Local Flow Field Properties over the Ground Plane and Rail (RT-3 Rail Tip,), M_∞ = 3.0 and Re_d = 1.8 × 10^6

8

The most pronounced disturbance generated in the flow field is located near the outer extremity of the upper rail surface above the ground plane ($Z = 2.0$ in.) at $Y = 1.5$ in. (see Fig. 4). In this area, there is an abrupt decrease in the local pitot pressure. This disturbance is present along that portion of the rail that lies on the ground plane. Upstream of the ground plane (for example, when $X_S = 9.6$ in.), this disturbance is not present. These results suggest that the disturbance is probably generated by an aerodynamic interference effect between the rail and ground plane surfaces.

A comparison of the disturbances produced by each of the three different rail tip configurations is shown in Fig. 5. Although the RT-2 rail tip configuration reduced the flow field disturbance near the upper rail surface, it also resulted in an increase in the disturbance over the ground plane. These results might suggest that the RT-2 rail tip configuration would have the least effect on the aerodynamic loading on the sled because a more uniform flow field exists in the vicinity of the upper rail surface. The variations in the flow field generated by the RT-2 and RT-3 rail tips would supposedly alter the local loading and flow field generated by the sled slippers. However, these local rail disturbances had a fairly small effect on the resulting sled force and moment coefficients, and this is illustrated in the following table.

TABLE II
TYPICAL RAIL EFFECTS ON SLED LOADING COEFFICIENTS

Coefficient	RT-3	RT-2*	Change, percent
C_N	0.318	0.305	-4.3
C_D	0.340	0.342	0.6
x_1/ℓ	0.195	0.195	0

$M_\infty = 3.0$, $X_S = 3.0$ in., and $X_R = 17.6$ in.

*These values were interpolated for $X_S = 3.0$ in.

Increasing the distance between the rail tip and the sled reduced the variation in these force coefficients; that is, increasing X_R reduced the percentage of change in the values listed in Table II.

Profile at 15.83 in. Aft of Ground Plane Leading Edge

Rail Tip at 17.63 in. Forward of Ground Plane Leading Edge

Solid Line - $M_L \sim 3.0$

Dashed Line - $M_L \sim 2.8$

RT-1

RT-2

RT-3

Rail ℄

RT-1

RT-2

RT-3

RT-1

RT-3

RT-2

Z, in.

Y, in.

Y = 1.50 in.

Sym	RT
□	1
△	2
○	3

Z, in.
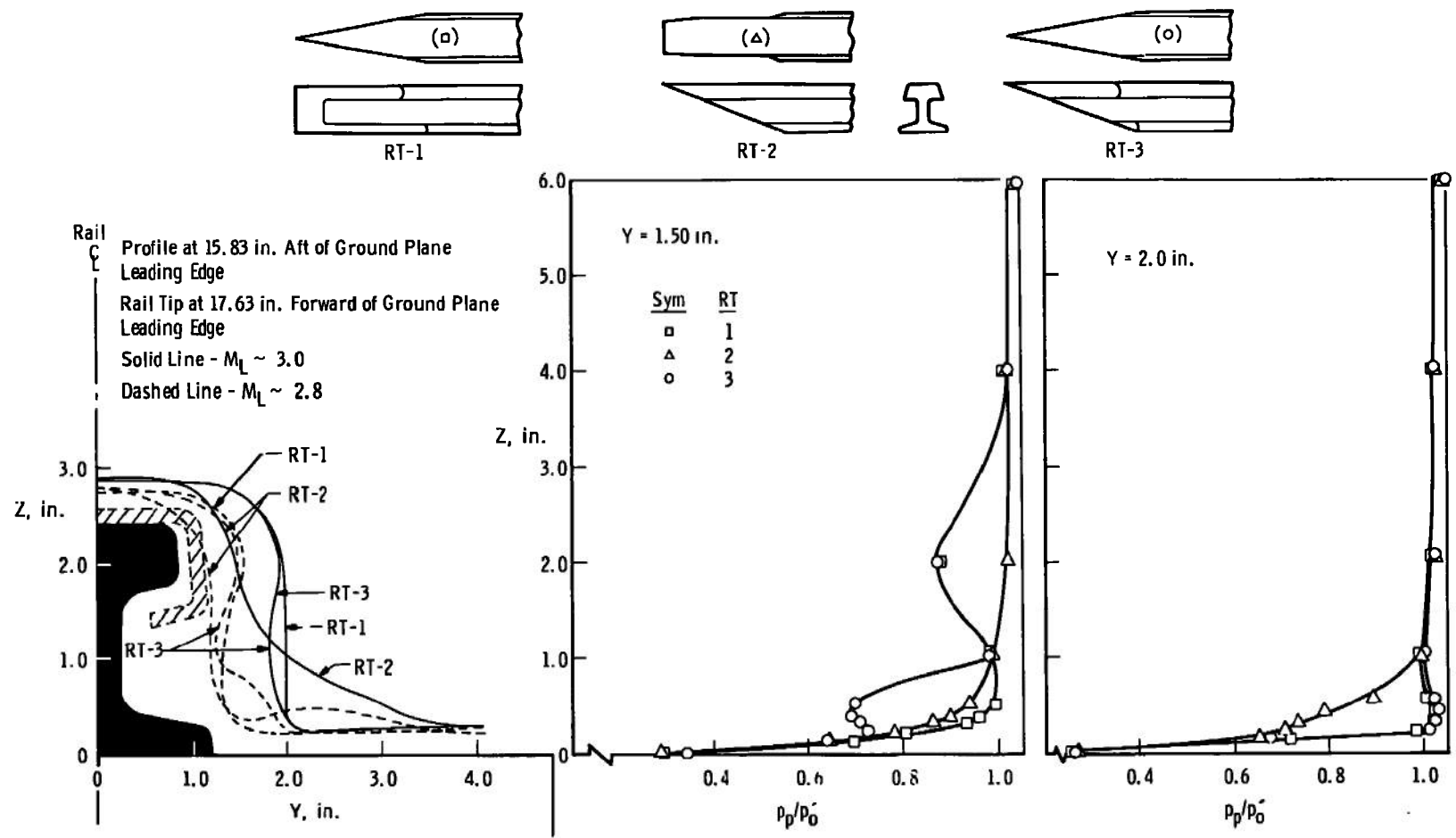
p_p/p_0'

Y = 2.0 in.

p_p/p_0'

Fig. 5 Rail Tip Effects on the Flow Field, $M_\infty = 3.0$ and $Re_d = 1.8 \times 10^6$

In view of the small differences noted in the sled loadings between the use of rail tips RT-2 and RT-3 it was decided to use RT-3 for these tests because of its better operating characteristics. An upward deflection of the rail caused by the aerodynamic loading of rail tip RT-2 necessitated realignment of the sled model on the rail and hence a significant change in the sled pitch attitude. Rail deflections with tip RT-3 were minor, and the axial loading on the rail drive system was also less with this tip configuration.

The flow survey results suggest that the boundary layer was thinner near the outer edge of the ground plane. Also, the pitot pressure and velocity profiles in the boundary layer indicate that the boundary layer on the rail and ground plane surfaces was turbulent in the region occupied by the sled. At the sled location of X_S = 3.0 in. and X_R = 17.6 in., the boundary layer on the rail at Mach number 3.0 was 0.23 in. thick. A summary of the bow wave locations and boundary-layer-thickness distribution over the rail and ground plane surfaces is shown in Fig. 6.
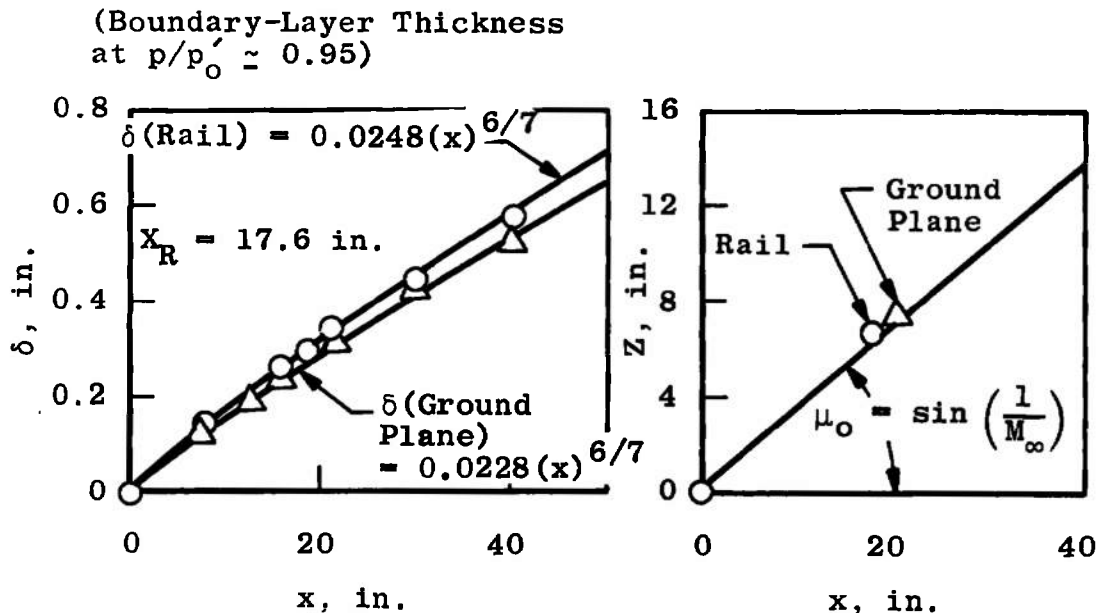
(Boundary-Layer Thickness
at $p/p_o' \simeq 0.95$)

Fig. 6 Summary of Flow Field Characteristics Generated over the Rail and Ground Plane, M_∞ = 3.0 and Re_d = 1.8 × 10^6

It can be seen that the bow wave angle for the rail tip and the ground plane leading edge is nearly equal to the free-stream Mach angle of 19.5 deg. The effect of model span on the variation in the ground plane bow wave location and on the variation of the boundary-layer thickness was negligible. Therefore, only nominal values of these parameters are shown in Fig. 6. Also, although not shown, the variation in the rail tip geometry had essentially no effect on either the bow wave location or on the boundary-layer thickness in the region to be occupied by the sled model.

A comparison of these wind tunnel results and the assumed full-scale track test environment suggests some basic differences in the flow fields as illustrated by Fig. 7. As previously noted, the local

a. Actual Track Environment
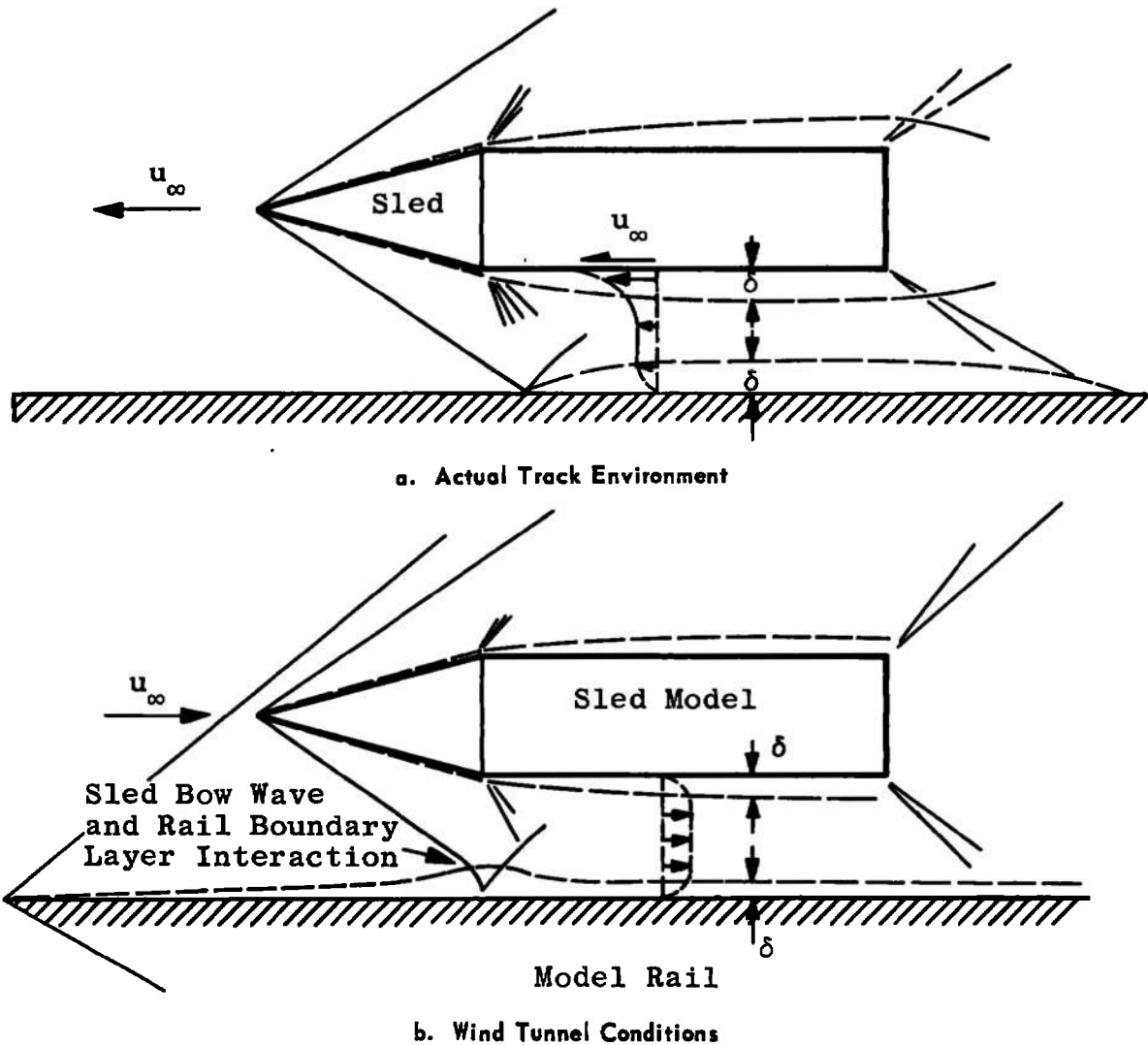

b. Wind Tunnel Conditions

Fig. 7 Comparison of Track and Wind Tunnel Test Environments

variations in the flow field produced by the different rail tips did not significantly alter the overall aerodynamic loading on the wind tunnel model. Of course, this does not eliminate the possibility that unwanted effects resulting from the presence of the boundary layer on the model rail will exist. For example, there is a separation effect resulting from the sled bow wave-boundary layer interaction on the rail which might influence the sled loading. In the case of the track environment, the sled bow wave is essentially unimpeded as it intersects the rail. The boundary-layer effects will also change the reflected shock pattern trapped between the sled and the rail. Only a comparison of track and

wind tunnel data will reveal the significance of these boundary-layer effects on the sled forces. However, one alternate procedure being considered for evaluating these effects in a wind tunnel test program is to remove the boundary layer from the rail surfaces. At Mach number 3.0, the flow field surveys indicated that the mass of air in the rail boundary layer to be removed upstream of the sled location is about 0.22 lb_m/sec.

3.2 MODEL ORIENTATION EFFECTS

3.2.1 Relative Location of the Sled and Rail Tip to the Wind Tunnel Model Ground Plane

Since the sled and rail tip could be moved independently of each other and relative to the ground plane, tests were made to determine which combination of rail tip and sled locations seemed to be ideal. In this case, the so-called "ideal" location was chosen as that where a variation of one or two inches in the sled and rail tip position did not produce any significant variations in the aerodynamic loads on the sled. The results of these tests are presented in Appendix III and summarized in Fig. 8. This figure shows the rail tip and sled locations which seemed to produce the least variation in the aerodynamic coefficients.
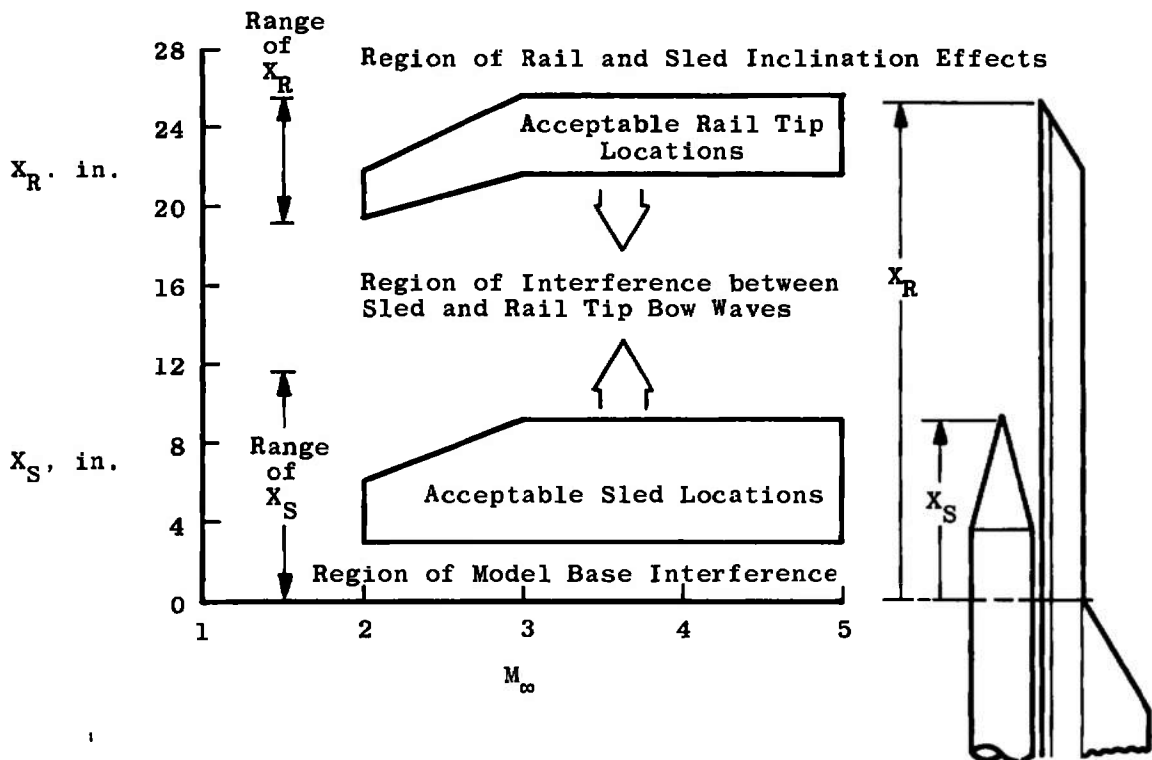

Fig. 8 Acceptable Model and Rail Tip Locations

As the sled configuration was retracted along the rail (that is, as $X_S \rightarrow 0$), there was a base flow interference effect produced when the model base was in proximity to the model support system. Therefore, any test data obtained for sled locations (X_S) less than 3.0 in. were susceptible to abrupt variations in the model base drag.

Another region of interference was generated as the sled approached the rail tip. In this case, the rail tip bow wave and flow field tended to disrupt the local flow field over the sled. Theoretically, the expansion fan emanating from the cone-cylinder shoulder of the sled model and the reflection of these waves from the bow wave of the sled create part of the aerodynamic loading on the aft portion of the sled. This loading will remain constant as long as the rail tip bow wave does not alter the flow field over the sled. In the present case, an intersection of the rail and sled bow wave forward of a point approximately midway along the body would tend to alter the sled loading. The variation of this intersection point with the free-stream Mach number is shown in Fig. 9. As this intersection point moves upstream, the rail tip disturbance tends to have a greater effect on the aerodynamic loading on the sled.
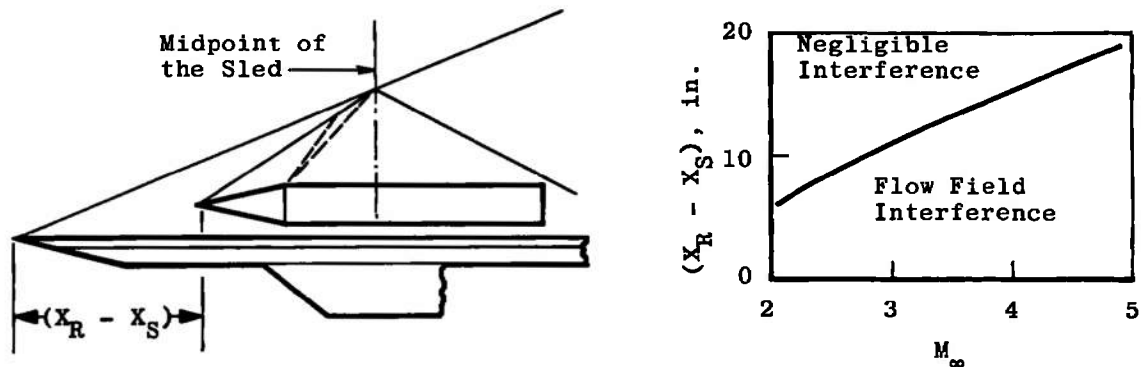

Fig. 9 Minimum Distance between Sled and Rail to Avoid Aerodynamic Disturbances

Extending the model rail or the sled model (that is, an X_R or X_S increase) usually resulted in a variation in the sled aerodynamic loading. Theoretically, extending the rail would produce a positive increase in pitching moment on the model support (deflection upward), but extending the sled would induce a rail and ground plane loading resulting in a negative pitching moment. During the test program, the entire model configuration tended to deflect negatively (less than 1 deg), indicating that the elements producing a negative pitching moment were more predominant. Therefore, the sled model which was normally aligned with the rail was also at a slightly negative free-stream angle of attack, and the test

results indicated that as the rail and sled were extended, the sled normal-force coefficient decreased. In some cases with the sled extended, the sled loading was influenced not only by the interference zone generated by the rail tip, but also by the model deflection angle of attack. This region in Fig. 8, which lies above the area of acceptable rail tip locations, was labeled as an area more likely to produce an undesirable angle-of-attack effect on the model.

3.2.2 Vertical Displacement of the Sled

Early in the test program, an effort was made to determine if a small displacement (less than 0.25 in.) in the sled away from the rail surface would have any effect on the sled aerodynamic characteristics. A fouling-light system attached to the forward and aft slippers was used to locate the sled and provided a consistent and fairly reliable way to position the sled above the rail.

Using two precision transit instruments, the sled was moved vertically and parallel to the rail surface. This movement produced some significant variations in the sled aerodynamic coefficients as shown in Fig. 10. The results were obtained with the slippers attached to the sled. This small increase in sled height (less than 0.140 in.) resulted in a 6-percent increase in drag, nearly a 30-percent decrease in the forward slipper normal force, and a 25-percent decrease in the aft slipper normal force. There was also a slight variation in the location of the resultant force vector with this small change in slipper gap size. These results emphasized the importance of maintaining a constant slipper gap when comparing test data obtained at various free-stream conditions.

In terms of model scaling with respect to the full-scale slipper gap, the present symmetrical model slipper gap was 2.5 times too large. There is a possibility that any differences that might arise between the wind tunnel and track (full-scale) test data may be attributed, in part, to this enlarged model slipper
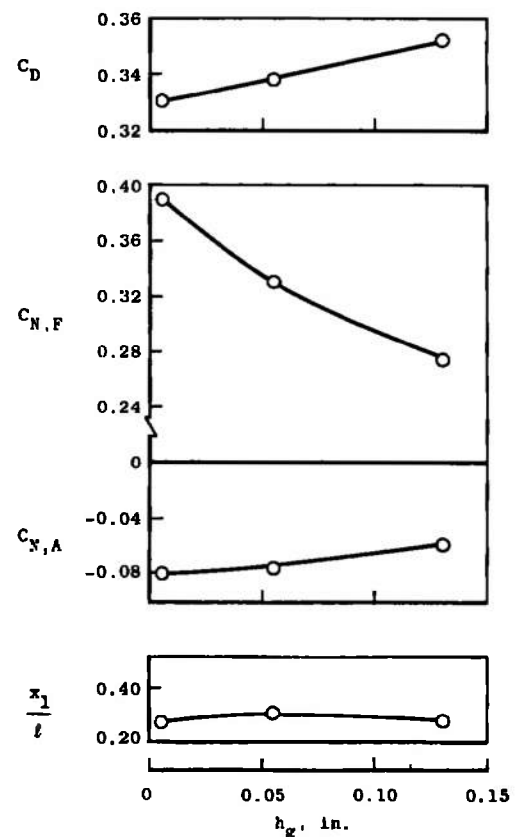
Fig. 10 Slipper Gap Variations, $M_\infty = 3.0$, Cone-Nose Sled

15

gap. With the present wind tunnel test equipment, the model slipper gap could probably be reduced without too many additional operational problems.

The gap between the rail and slipper was held to within 0.005 in. for all subsequent "slipper-on" test results. For the "slipper-off" test data, a similar gap existed between the slipper support and the slipper which was attached to the rail.

The test data obtained with the slippers off were used to define experimentally the aerodynamic loading imposed on the slipper supports. On the full-scale vehicle, these supports will be instrumented with strain gages to monitor the loading transmitted to the slipper shoes by the sled body. The slipper-on data represent the forces imposed on the slipper at the point where the slippers are in contact with the rail. The difference between the two slipper configurations (that is, slipper-on versus slipper-off) is considered to be representative of the aerodynamic loading which may be ascribed to the slippers.

Two additional model configurations were tested which consisted of displacing the sled body from the rail surface by inserting larger supports between the sled and the slippers. Increasing the height of the sled above the rail also increased the frontal area of the sled and, therefore, resulted in a significant increase in drag as shown in Fig. 11. The aerodynamic coefficients in Fig. 11 are all referenced to the sled frontal area and, therefore, the reference area is a function of the sled height. Although there is a slight variation in the increment of drag coefficient attributed to the sled slippers (that is, the difference in C_D values for slippers on and slippers off), this incremental drag coefficient variation, when evaluated in terms of a constant reference area, indicates that the slipper drag coefficient is independent of the sled height (h).

The theoretical analysis of Ref. 2 indicates that as the sled is displaced from the ground surface the resultant normal-force coefficients (that is, $C_{N,A} + C_{N,F}$) should decrease. This predicted trend in the normal-force coefficient ($C_{N,A} + C_{N,F}$) is substantiated by the data in Fig. 11. The incremental increase in normal force attributed to the slipper (that is, the slipper-on minus the slipper-off data) tended to decrease slightly as the sled height increased. Also, the addition of the slipper to the sled shifted the location of the resultant force vector downstream toward the forward slipper (that is, x_1/ℓ decreased).

A comparison of the drag and normal-force coefficient rates of change with sled height (h) near $h/d = 0.57$ is essentially equal to the rates of change produced by varying the slipper gap height (h_g). This

comparison again indicates the importance of the gap height (h_g) as well as sled centerline height (h), relative to the rail, when comparing various monorail data.
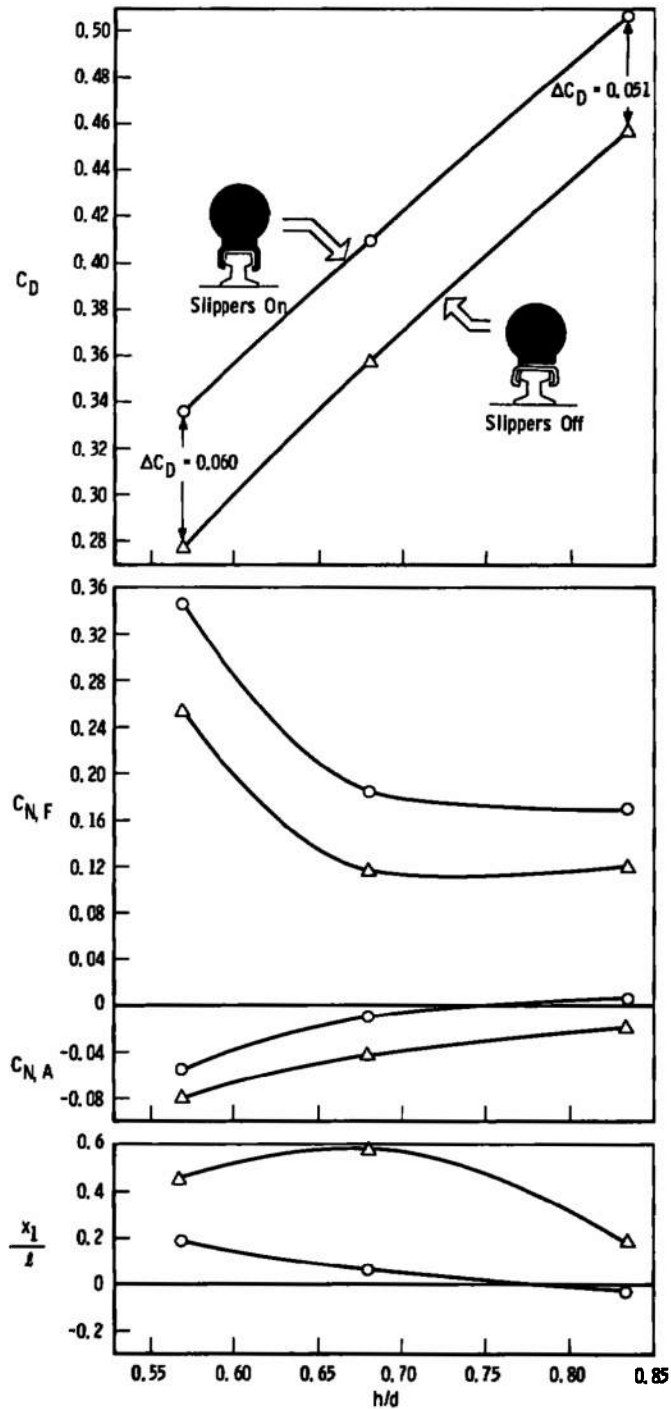

Fig. 11 Sled Height Variation, M_∞ = 3.0, Cone-Nose Sled

3.2.3 Roll Stability

The variation of the aerodynamic coefficients with angle of roll is given in Appendix III (Fig. III-2). In general, a 4-deg variation in the angle of roll had negligible effects on the drag, normal-force, and pitching-moment coefficients. The rolling-moment and side-force coefficients increased slightly with the angle of roll. The basic data shown in Fig. III-2 show that there is a shift in rolling-moment, side-force, and yawing-moment coefficients at zero roll. This shift may be attributed to the observed small misalignment of the sled and slippers in the yaw plane, relative to the rail axis.

The aerodynamic roll stability of the sled is shown in Fig. 12. In this case, the rolling-moment coefficient is referenced to the hypothetical contact point between the sled slipper and the rail as the sled rolls. This contact point (Q) is assumed to be located at the outer rim of the upper surface of the rail (0.80 in. from rail centerline). These results indicate that the sled is unstable if the restoring moment produced by the sled weight is less than the aerodynamic rolling moment shown in Fig. 12. The abrupt change in sign of the rolling-moment coefficient at zero roll is caused by the corresponding change in the hypothetical contact or moment reference point as the sled roll angle changes sign. Also, these results suggest that the slipper loading is responsible for most of this aerodynamic static roll instability.
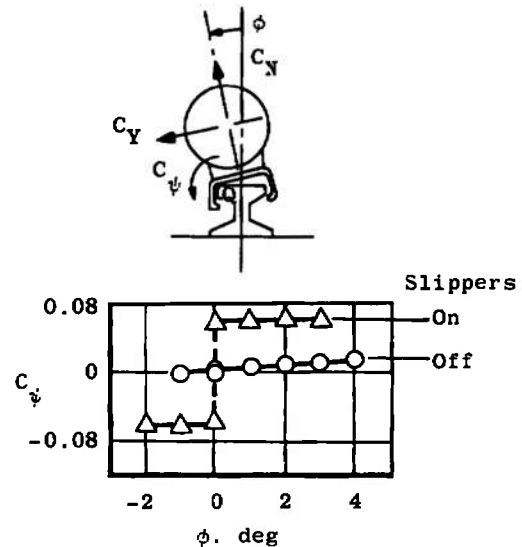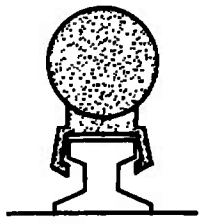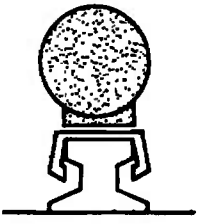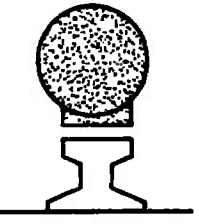

Fig. 12 Roll-Angle Effects on Sled Stability, $M_\infty = 3.0$

3.2.4 Slipper Effects

In past monorail wind tunnel tests, the slippers have been omitted from the model configuration. The present results indicate that the slippers account for a significant part of the overall aerodynamic loading on a sled. This slipper influence on the aerodynamic coefficients is illustrated by the Mach number 3.0 data in Table III.

TABLE III
MONORAIL SLIPPER EFFECTS

Model Configuration			
Slippers	On	Off	Removed
Coefficient			
C_N	0.261	0.174	0.086
C_m	0.043	0.069	0.080
C_D	0.341	0.277	0.293
$C_{N,F}$	0.314	0.254	0.189
$C_{N,A}$	-0.053	-0.080	-0.103
x_1/ℓ	0.200	0.459	1.205
$M_\infty = 3.0$, $Re_d = 1.8 \times 10^6$, and $h = 2.0$ in.			

This table clearly demonstrates that wind tunnel monorail sled test results obtained without slippers are not likely to correlate very well with full-scale track data.

3.3 REYNOLDS NUMBER AND BOUNDARY-LAYER TRIP EFFECTS

The environment produced by the full-scale sled as it moves along the track will approach a free-stream Reynolds number (Re_d) of 13 million at Mach 3.0. At this Reynolds number, the boundary-layer flow over the sled body is predominantly turbulent. In the wind tunnel tests, the Reynolds number is less than 2 million, and the flow over the sled is primarily laminar or transitional. Therefore, an investigation was made at a free-stream Mach number of 3.0 to determine the smallest boundary-layer trip required to produce turbulent flow over the wind tunnel model. These boundary-layer trips were placed only on the cone- and spike-nose sled configurations on the forward shoulder of the cylindrical body, on the slippers, and on the splitter wedge upstream

of the slippers. The influence of the boundary-layer trip size (ϵ) at various free-stream Reynolds numbers is shown in Fig. 13.

If the flow is predominantly laminar over the sled surface, an increase in grit size produces an increase in the forebody drag coefficient (C_D) as shown by the data obtained at $Re_d = 0.22$ million in Fig. 13. This increase in drag is usually attributed to an increase in the aerodynamic frictional drag of the sled as a greater portion of the flow over the sled becomes turbulent. Eventually, over a limited range of grit sizes, the drag coefficient is fairly insensitive to a variation in the grit size, and the flow over the body is assumed to be predominantly turbulent for the data obtained at $Re_d = 1.1$ and 1.8 million (Fig. 13).

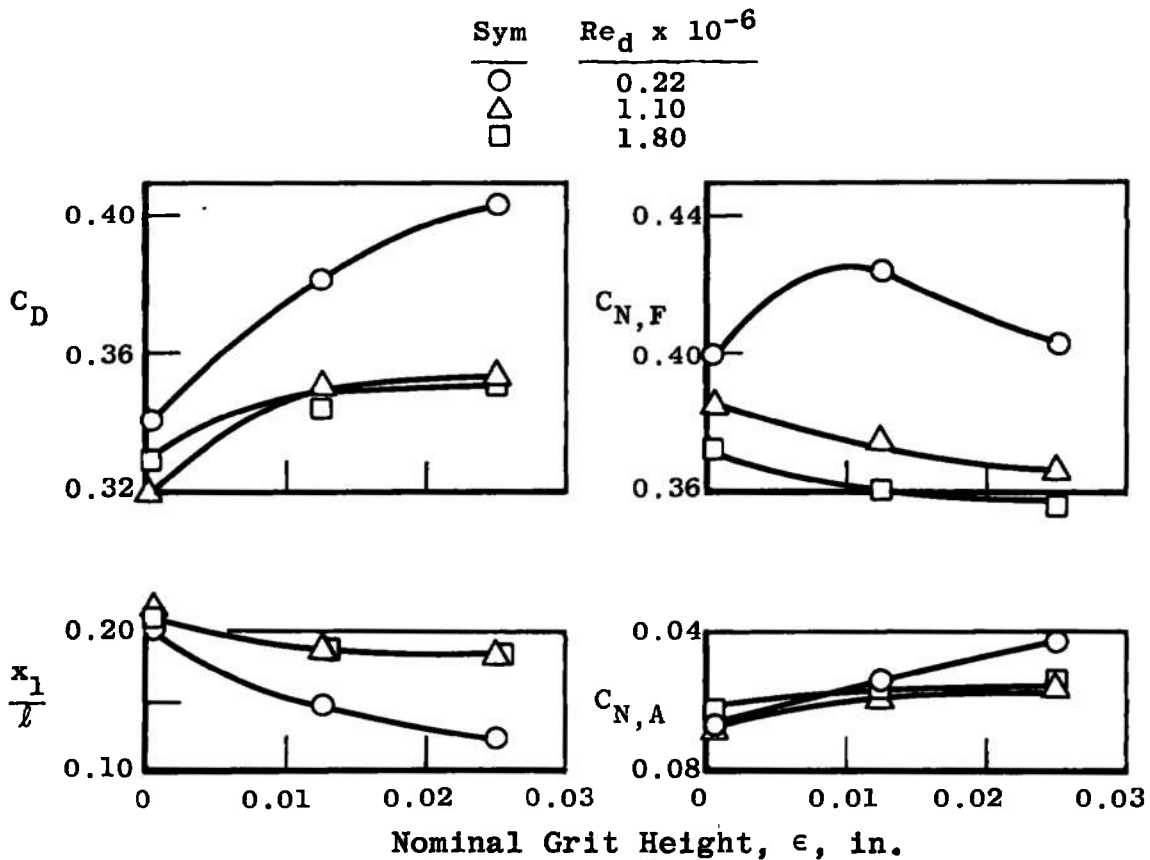| Sym	$Re_d \times 10^{-6}$
O	0.22
△	1.10
□	1.80

Fig. 13 Reynolds Number and Boundary-Layer Trip Effects on the Cone-Nose Sled with Slippers On

The variations in the drag coefficient produced by the boundary-layer trips also influenced the slipper loading coefficients ($C_{N,F}$ and $C_{N,A}$) and the location of the resultant sled force vector (x_1/ℓ). When a variation in grit size failed to affect the drag coefficient, the sled

slipper loads and moments also became fairly insensitive to the variations in the grit size. These limited boundary-layer trip results indicate that a grit size between 0.015 and 0.025 in. would be adequate for the present sled tests in the Reynolds number range from 1.1 to 1.8 million at Mach number 3.0.

The variation in Reynolds number had some effect on the aerodynamic coefficients of the cone-nose sled configuration at the lower free-stream Mach numbers as shown in Fig. 14 for $M_\infty = 3.0$. A logarithmic extrapolation of the Mach number 3.0 data (that is, log $(C_{N,F})$ or log (C_D) versus log (Re_d) was made to the full-scale vehicle Reynolds number of 13 million. This extrapolation indicated that, relative to the wind tunnel results obtained at a Reynolds number of 1.8 million with roughness, the full-scale vehicle drag and normal-force coefficients would be 3 or 4 percent lower.
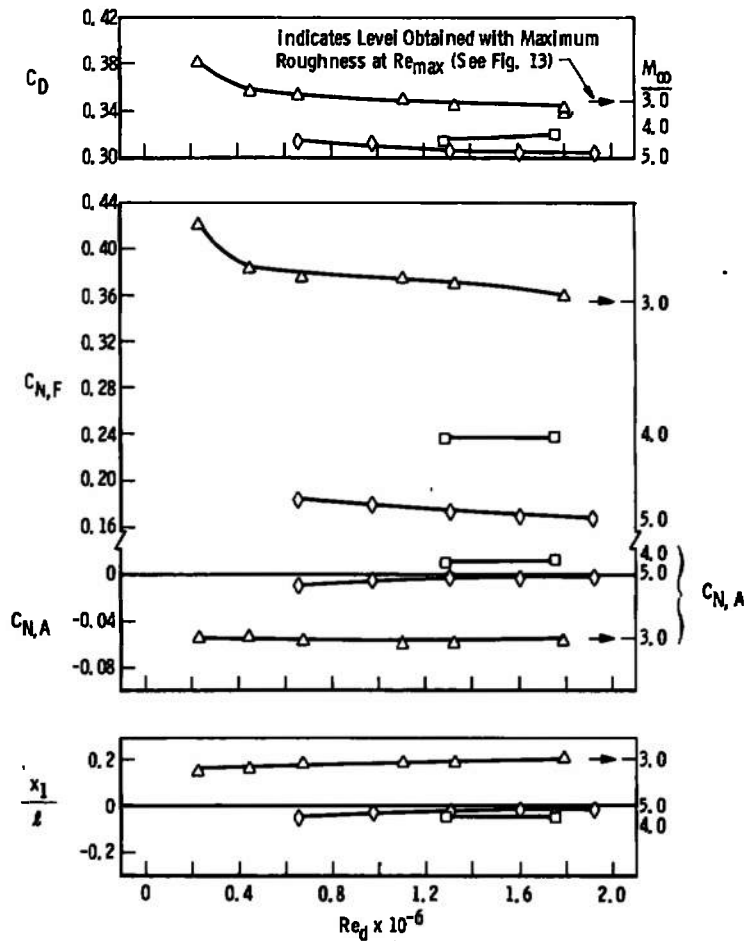
Fig. 14 Reynolds Number Effects on the Cone-Nose Sled with Slippers On

   This estimated 3- or 4-percent difference in drag coefficient based
on the previous Reynolds number extrapolation between the wind tunnel
model and the full-scale vehicle is nearly equal to the predicted change
in drag attributed to the differences in the turbulent aerodynamic fric-
tional drag of these bodies. Figure 15 contains estimates of the turbu-
lent skin friction drag coefficient of the wind tunnel model and full-scale
vehicle and also estimates of the laminar skin friction drag coefficient
of the wind tunnel model. The difference between the turbulent skin
friction drag coefficient curves at Mach number 3.0 is about 0.009.
This difference represents a little less than 3 percent of the resultant
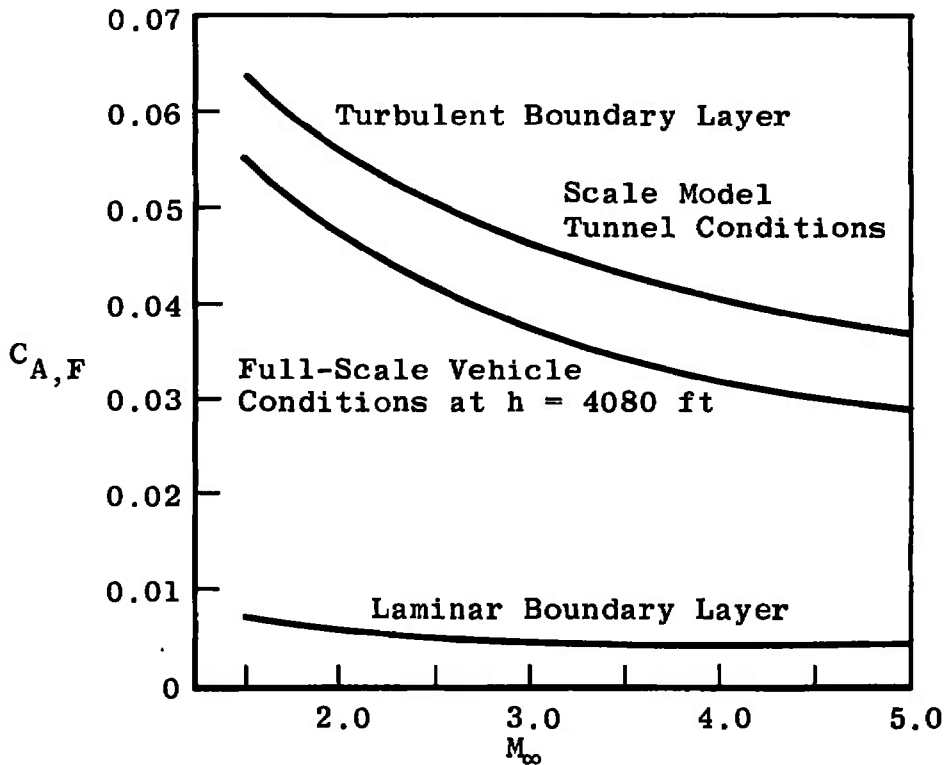forebody drag coefficient of the wind tunnel model.

Fig. 15 Skin Friction Drag Estimates

   In the case of the spike-nose sled, particularly at the lower Mach
numbers ($M_\infty < 4.0$), the Reynolds number effect on the aerodynamic
loading of the sled was more pronounced as shown in Fig. 16. At each
free-stream Mach number, there is a particular critical Reynolds num-
ber where a slight increase or decrease in Reynolds number resulted
in an abrupt change in the sled drag coefficient. This change in drag
was caused by an abrupt change in the separated flow over the spike as
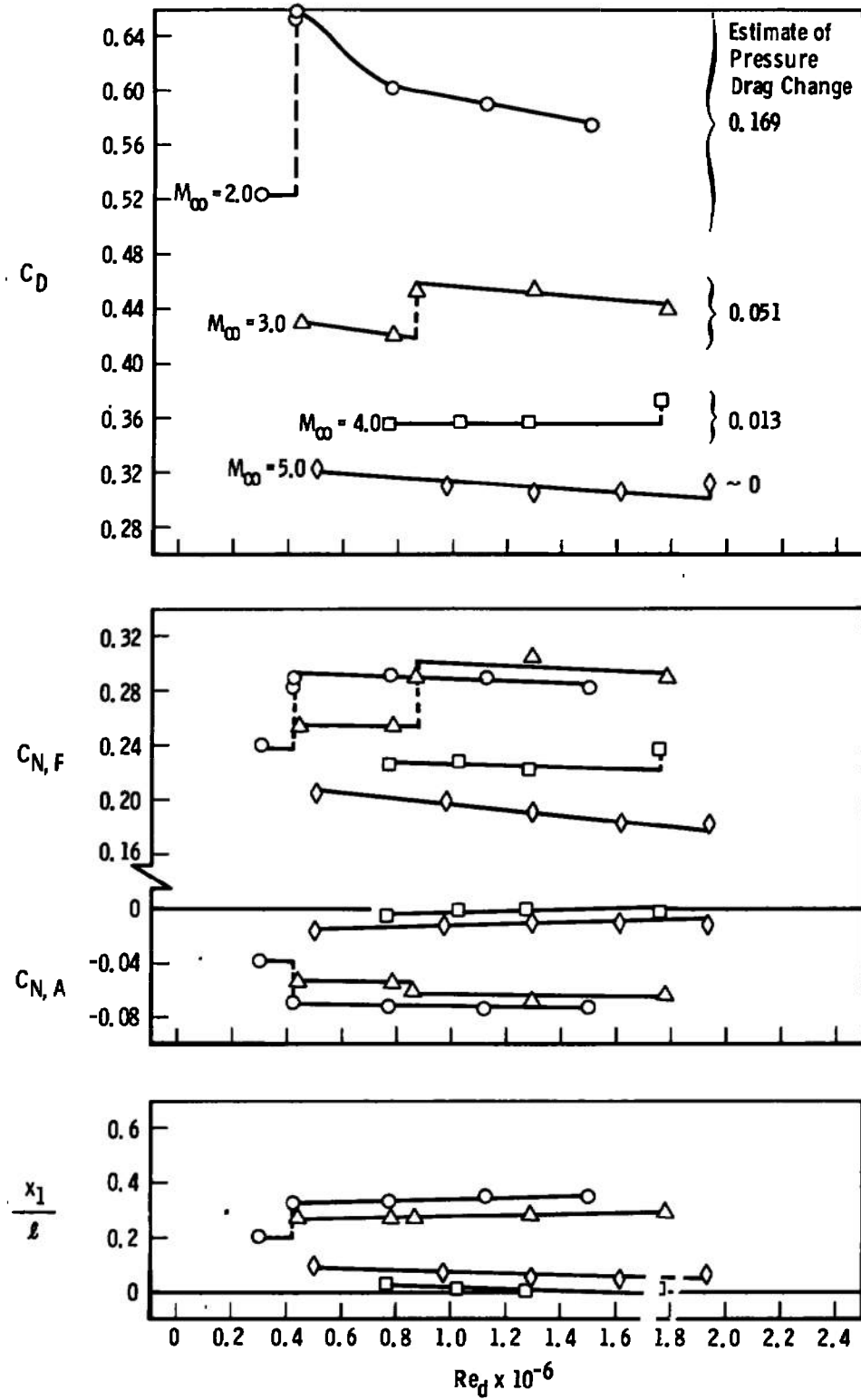illustrated in Fig. 17.

Fig. 16 Reynolds Number Effects on the Spike-Nose Sled with Slippers On

The separation results in Fig. 17 were used to estimate the change in pressure drag on the cylindrical afterbody. The assumption was made that the region of separated flow acted as a conical body and that the separation angle could be related to the surface pressure ratio for a cone. The estimated changes in pressure drag based on the change in the separation lengths are indicated in Fig. 16. Although these crude estimates exceed the pressure drag change at the lower free-stream Mach number, the estimated trend in the pressure drag with Mach number agrees with the experimental results.

Although there may have been some hysteresis in the separation phenomenon, a slight increase in Reynolds number near the critical value at Mach numbers 2 and 3 resulted in an abrupt shortening of the length of separated flow from the values plotted in Fig. 17. At the higher Mach numbers (4 and 5), the region of separation appeared to fluctuate at the critical Reynolds number so that the separation point moved about the locations shown in Fig. 17.

At the lower free-stream Reynolds number, the separated boundary layer enveloped the entire length of the spike at all Mach numbers from 2 to 5. The effective cone angle defined by this region of separation was about 13.3 deg. This separation angle increased abruptly when the free-stream Reynolds number was increased beyond the critical value (that is, when the boundary layer at the separation was predominantly turbulent).

At the maximum Reynolds numbers, the length of the separated flow at Mach numbers above 2 is primarily influenced by the characteristics of a separating turbulent boundary layer. The Mach number 2 schlieren photograph shows that a strong bow wave produced by the cylindrical afterbody of the sled probably provided an additional factor that increased the length of separated flow. This cylindrical afterbody bow wave was not as clearly evident in the higher Mach number schlieren photographs.

3.4 FLOW FIELD DISTURBANCE ON THE SLED BODY

It is shown later that theoretically a clean configuration of the present cone-cylinder sled model (that is, with the splitter wedge, slipper supports, and slippers removed) would produce an aerodynamic loading that would force the sled toward the rail. Experimentally, the sled configuration with the splitter wedges and slippers produced an aerodynamic loading that tends to pitch the sled nose up and away from the rail. One reason for this nose-up aerodynamic loading is suggested by the flow field disturbance produced primarily by the splitter wedge as shown in Fig. 18.
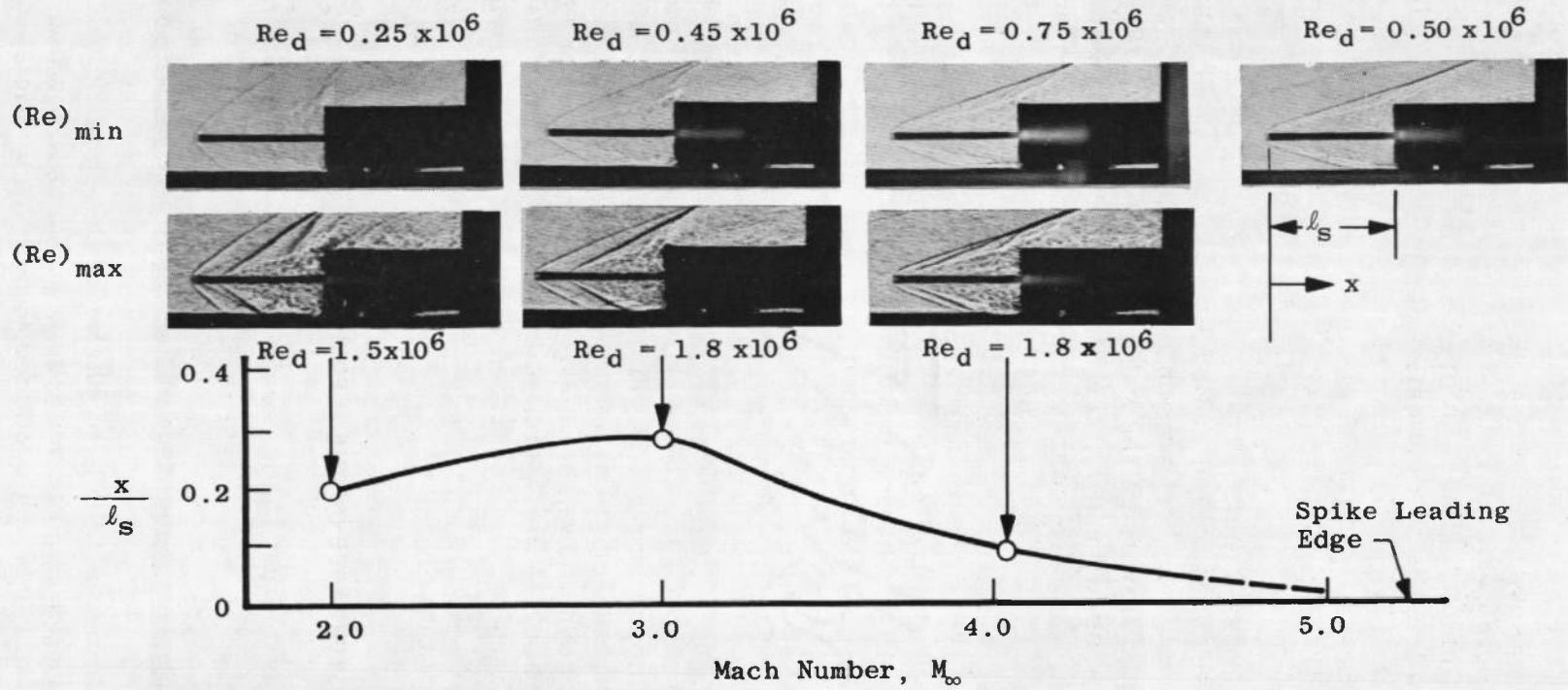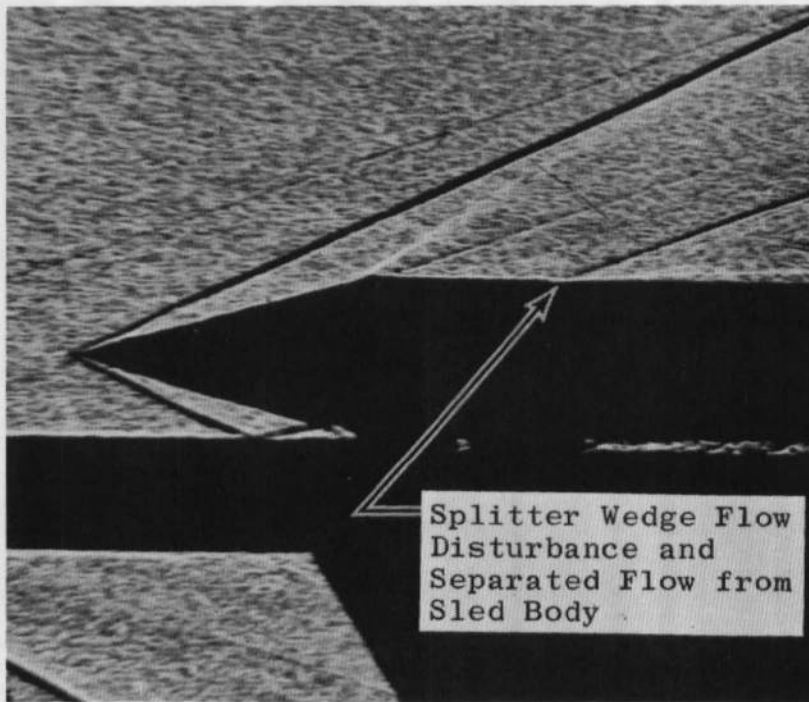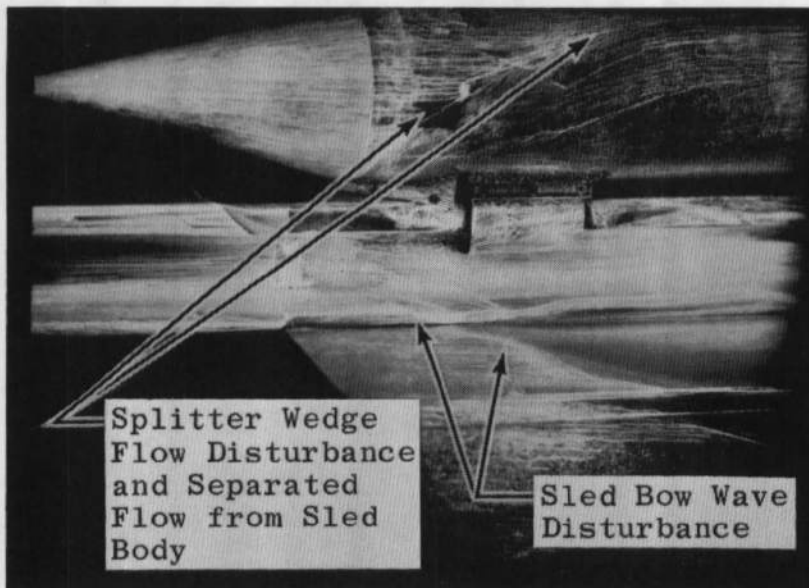
Fig. 17 Boundary-Layer Separation Location on the Spike Nose of the Sled

a. Shadowgraph

b. Oil Flow

Fig. 18 Typical Flow Field Pattern over the Cone-Nose Sled
$\left(M_\infty = 3.0, h/d = 0.57, \text{ and } Re_d = 1.8 \times 10^6\right)$

The splitter wedge shown in Fig. 18b produces a strong disturbance which originates underneath the sled body and wraps around the cylindrical section of the sled. This region of high pressure generated in the immediate region of the wedge would tend to push the sled away from the rail. Although not shown, a similar flow field pattern exists at the splitter wedge located upstream of the aft slipper.

The forward splitter wedge disturbance consisting of compression waves and wake flow moves aft along the cylinder and eventually propagates to the upper surface of the body. This disturbance probably causes the boundary-layer flow over the cylindrical surface of the sled to separate. As illustrated by the schlieren pictures in Fig. 19, the leading edge of the splitter wedge wake flow as projected on the upper surface of the sled moves upstream as the free-stream Mach number increases. Although this disturbance as observed in the schlieren pictures might represent a separation of the boundary layer from the sled, this location, not shown as a function of Reynolds number, was not influenced by variations in the free-stream Reynolds number (Re_d) of from 0.2 to 1.8 million.

A similar splitter wedge disturbance existed on the spike-nose configuration as shown in Fig. 20a. A comparison of the spike- and cone-nose splitter wedge disturbances indicates that the disturbance propagated farther downstream on the spike-nose configuration before reaching the upper surface of the cylindrical body of the sled (compare Figs. 20a and b).

Of course, the splitter wedge disturbance is only partly responsible for the loading that lifts the sled away from the rail. The force measurements also indicated that a significant part of the sled lifting force can be attributed to the slippers.

3.5 FREE-STREAM MACH NUMBER EFFECTS

The variation in the basic aerodynamic coefficients with the free-stream Mach number for the 15-deg cone- and spike-nose sled configurations is presented in Figs. 21 and 22, respectively. The "a" parts of these figures contain the wind tunnel results obtained at the maximum free-stream Reynolds number with boundary-layer trips on the sled model. At each test condition, the sled was aligned parallel to the rail surface with the sled axis located at an h/d value of 0.57 above the rail surface. The "b" parts of Figs. 21 and 22 represent the estimated loadings on the full-scale vehicle as defined by the aerodynamic coefficients in the "a" parts of these figures. The significance of the slipper-on and slipper-off data which correspond to the sled slipper loads and sled slipper support loads respectively in Figs. 21 and 22 is discussed in Section 3.2.2.
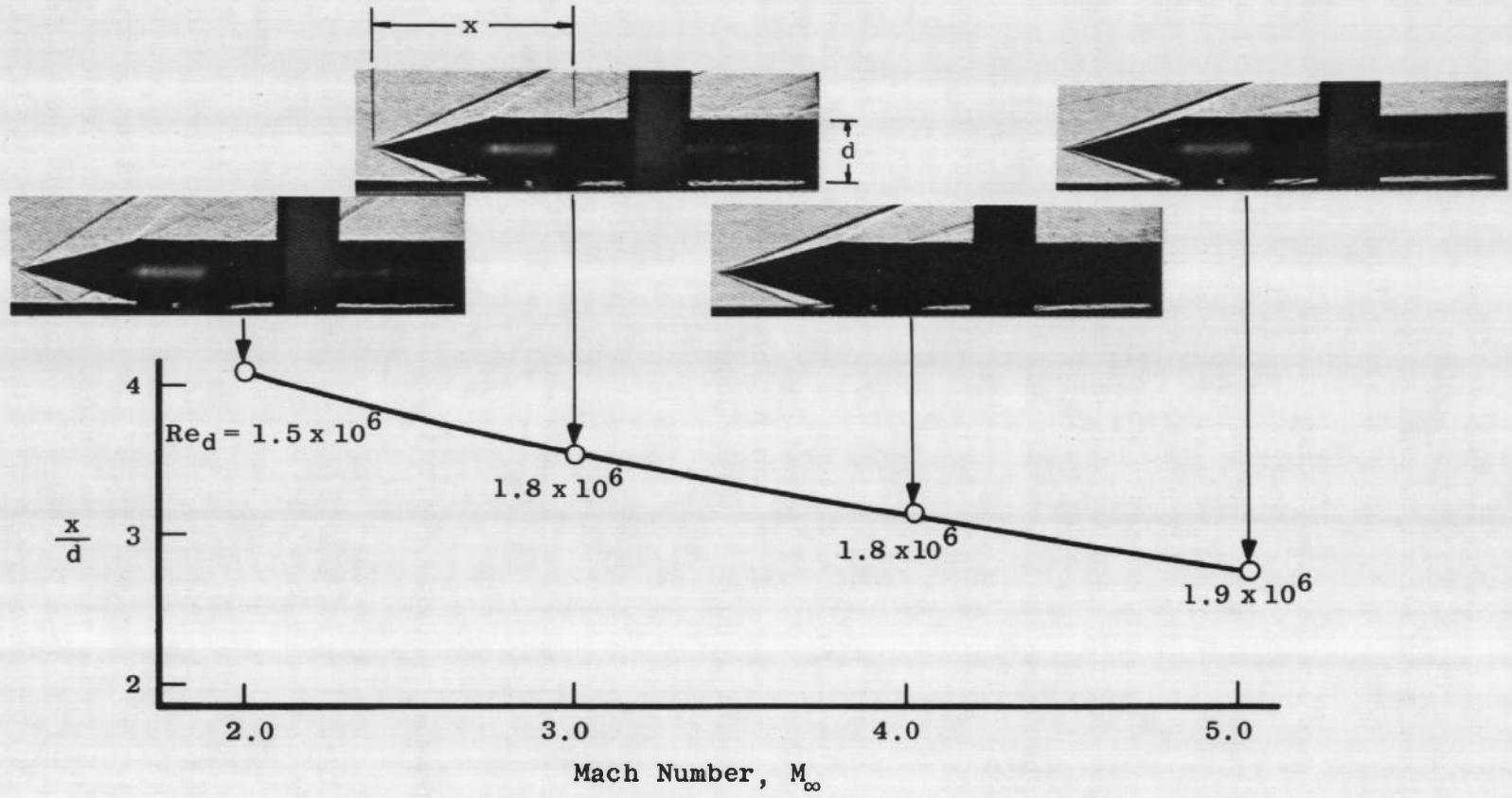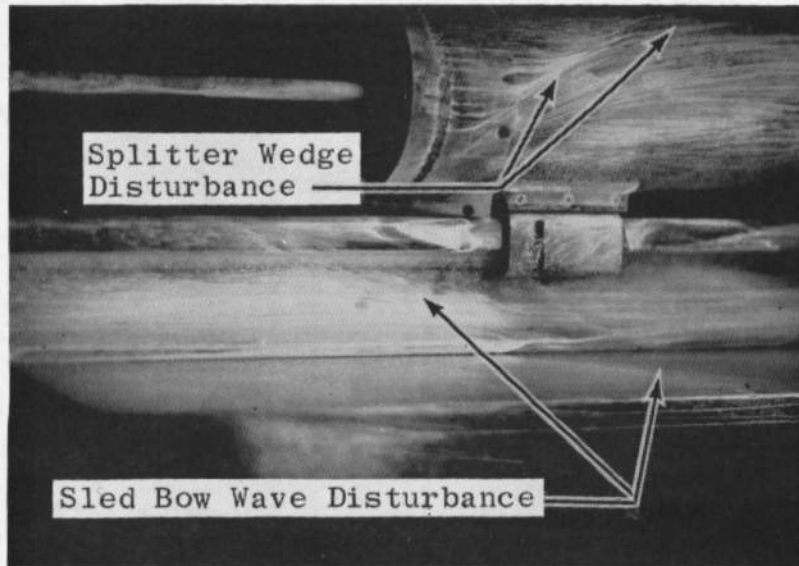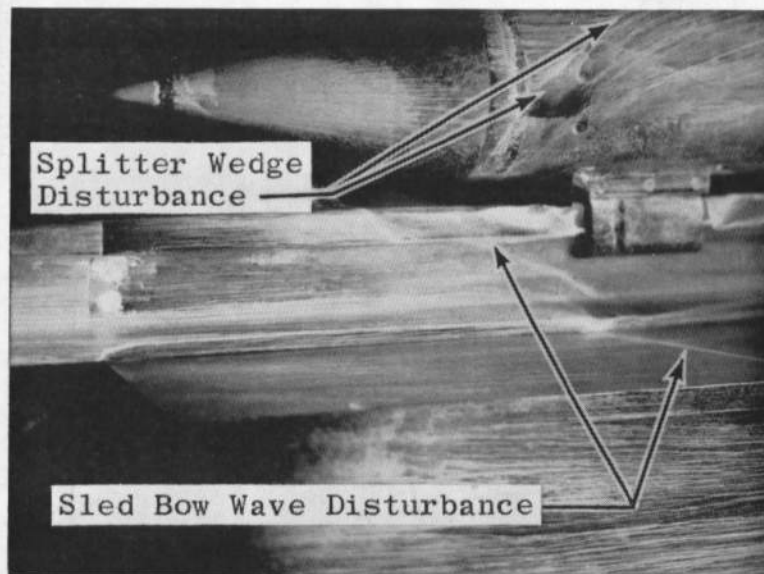
27

Fig. 19 Origin of the Splitter Wedge Wake Flow as Projected on the Upper Surface of the
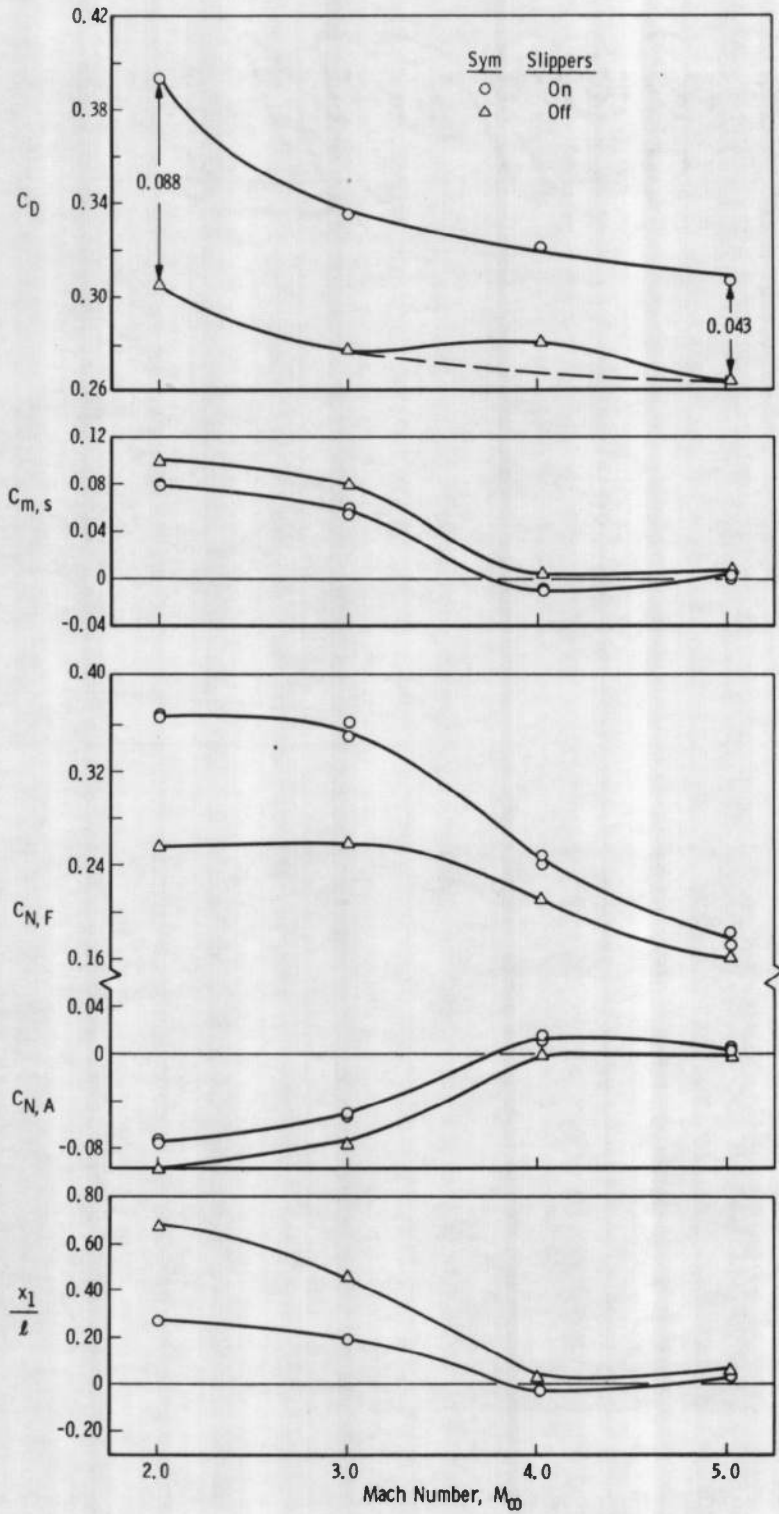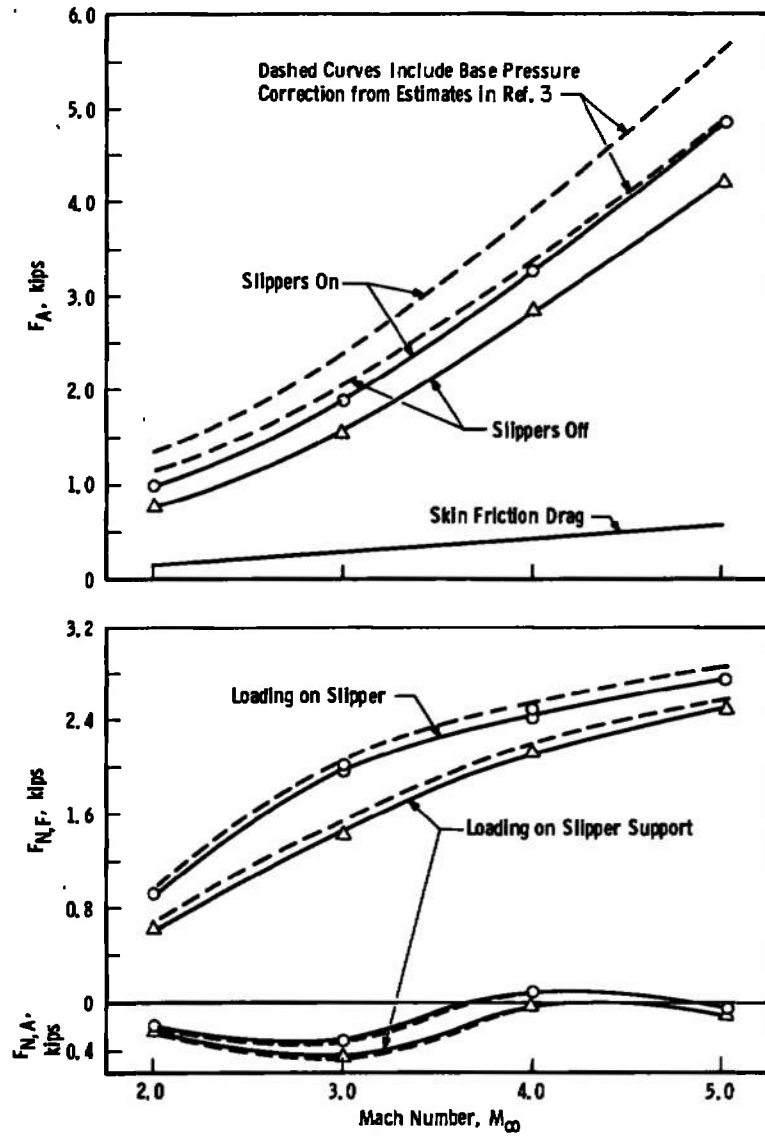Cylindrical Body of the Cone-Nose Sled

a. Spike Nose

b. Cone Nose

Fig. 20 Influence of the Nose Configuration on the Flow Field Disturbance over the
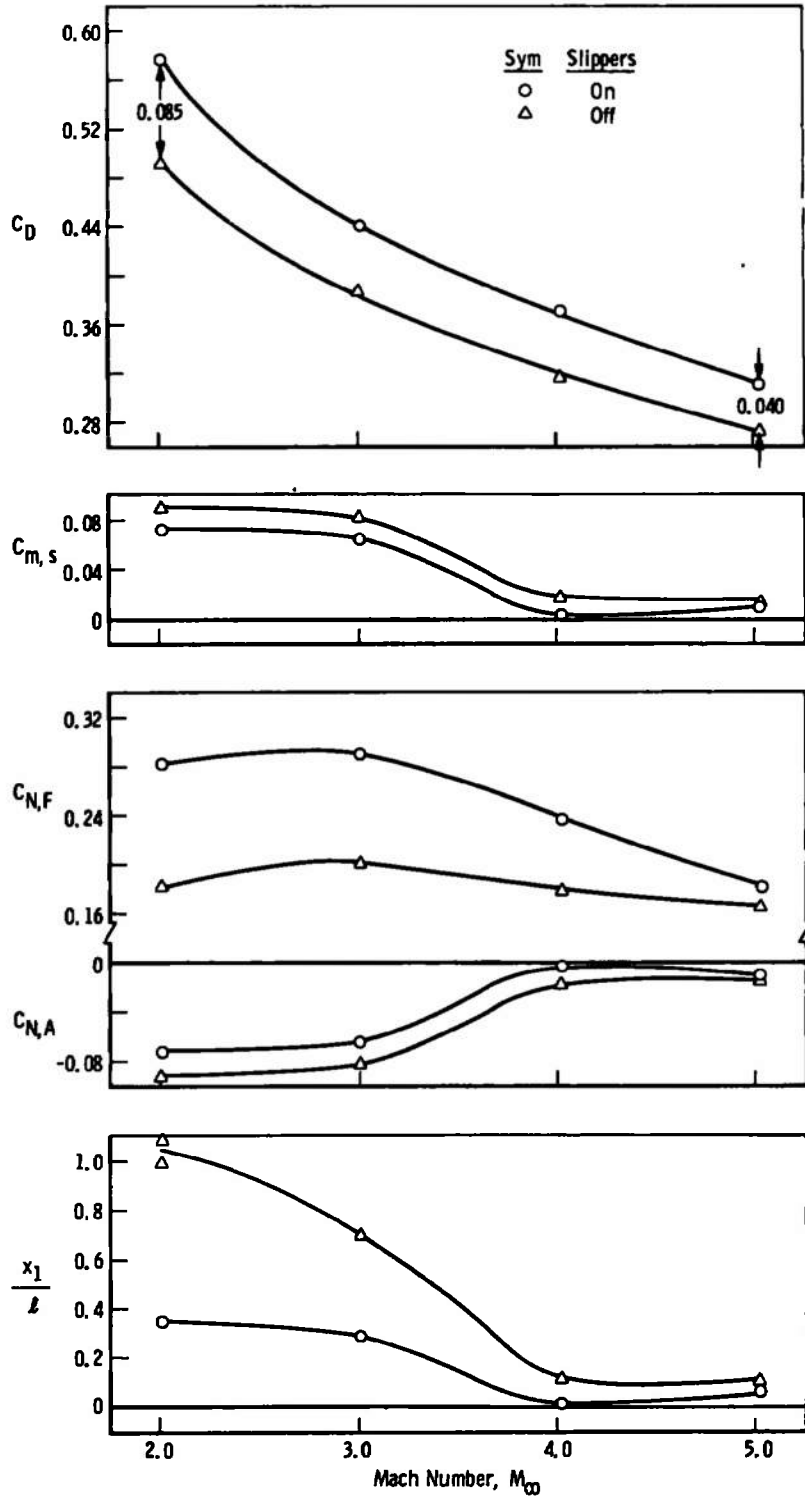Sled (M_∞ = 4.0, h/d = 0.57, and Re_d = 1.8 × 10⁶)

a. Wind Tunnel Model Coefficients (Maximum Re_d)

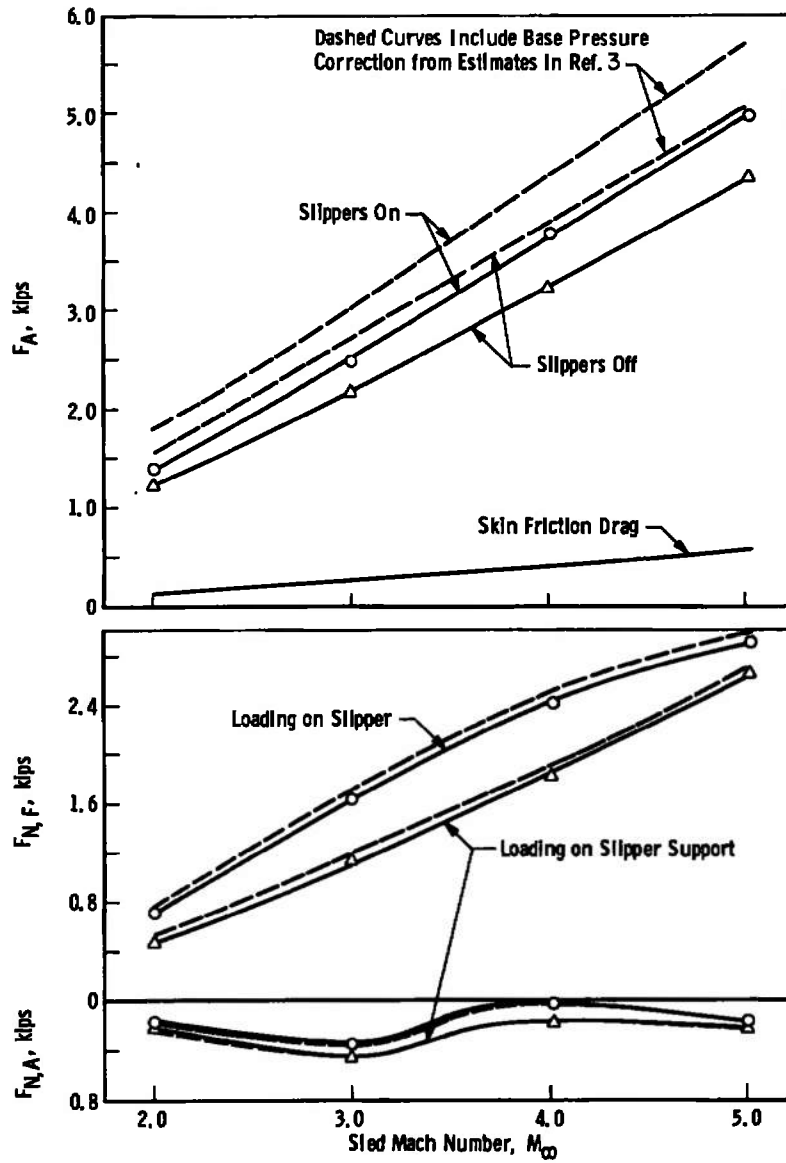Fig. 21 Aerodynamic Loading on the 15-deg Cone-Nose Sled $(h/d = 0.57)$

b. Estimated Full-Scale Loads
Fig. 21 Concluded

a. Wind Tunnel Model Coefficients (Maximum Re_d)

Fig. 22 Aerodynamic Loading on the Spike-Nose Sled (h/d = 0.57)

b. **Estimated Full-Scale Loads**
Fig. 22 Concluded

As expected, these results show that the forebody drag coefficients, particularly at the lower free-stream Mach numbers, are significantly larger on the spike-nose sled than on the cone-nose sled (compare Figs. 21a and 22a). This difference in the drag coefficient decreased with increasing Mach number. Except for the Mach number 4.0 data, the incremental change in drag produced by detaching the slippers from the sled was approximately the same for both the cone- and spike-nose sled configurations. These comparisons of the slipper effects on the drag coefficient suggest that the Mach 4.0 drag coefficient obtained for the cone-nose sled with slippers off (Fig. 21a) is unreasonably high. Therefore, an estimate of the correct drag coefficient is shown by the dashed curve in Fig. 21a.

The normal-force coefficients for the forward and aft slippers of both nose-sled configurations decreased with increasing free-stream Mach number. The most significant change in these coefficients occurred between Mach numbers 3 and 4, where there was a significant aft movement in the location of the resultant force vector along an axis passing through the sled slippers (that is, towards the forward slipper). At free-stream Mach numbers less than 4.0, the forward slipper normal-force coefficients of the spike-nose sled are significantly smaller than those of the cone-nose sled. The aft normal-force coefficient, $C_{N,A}$, and the pitching moment about the sled reference, $C_{m,s}$, were the same for the spike- and cone-nose configurations over the Mach number range tested. Thus, the best or smallest slipper loadings obtained over the Mach number range from 2 to 5 were obtained with the spike-nose sled configuration.

The estimated forebody drag force and slipper loadings on the full-scale vehicles (the cone- and spike-nose configurations) moving along a track at speeds in the Mach number range from 2 to 5 in an atmospheric environment equivalent to an altitude of 4000 ft are shown in Figs. 21b and 22b. These estimates are based on the measured wind tunnel model coefficients and have not been adjusted to account for the differences between the wind tunnel and full-scale Reynolds numbers.

Included in these figures is an estimate of the variation with Mach number of the frictional component of the forebody drag of the sleds. In general, the frictional drag represents about 10 percent of the sled forebody drag. Based on the previously estimated influence of the wind tunnel and full-scale Reynolds number on the frictional drag coefficient (see Section 3.3), these estimates of the full-scale forebody drag may be 3 or 4 percent high.

The normal-force coefficients obtained with the slippers off were used to provide a direct estimate of the loading imposed on the slipper support block of the full-scale vehicle. The forward slipper support loading on the cone-nose sled varied from 600 lbf at Mach number 2 to nearly 2500 lbf at Mach number 5. The loading on the aft slipper support remained below 450 lbf over this entire Mach number range.

Another factor that will alter these estimates of the drag and slipper loads is the estimated value of base drag on the full-scale vehicle. In the full-scale load estimates, the base pressure is assumed to equal the free-stream ambient pressure. Assuming the base pressure coefficient on the full-scale vehicle is equal to the values presented in Ref. 3 (Fig. III-4) for turbulent boundary-layer flow over bodies of revolution, the estimated correction to the forebody drag coefficient and the slipper loading coefficients for the full-scale vehicles are shown as the dashed curves in Figs. 21b and 22b.

The addition of the base drag represents a significant increase (as much as 36 percent at Mach number 2.0) in the drag coefficient of the sled. Actually, the full-scale drag force on the cone-nose sled at Mach number 2.0 would be 360 lbf higher; at Mach number 5.0, 850 lbf higher. These changes in sled drag will increase the forward slipper loads by 37 lbf at Mach number 2.0 and by 810 lbf at Mach number 5.0. Therefore, the influence of the base drag on the overall drag and slipper loads of the sled becomes more significant at the higher sled track speeds (i. e., at Mach numbers above 2.0).

An attempt was made to correlate the resultant lift force produced by the cone-cylinder sled configuration. The results of the correlation and a comparison of the test data with the theoretical estimates are shown in Fig. 23. The theoretical estimates as formulated in Ref. 2 (which assumes $M \gg 1$, $h^* < 1$, and $x_n/x_o < 1$) must be applied to a simple cone-cylinder body moving in proximity to the ground. Thus, the theoretical estimates neglect the disturbances produced by the sled splitter wedges and slippers. Theoretically, the simple cone-cylinder configuration moving in proximity to the ground would produce a negative lift force, but the experimental configuration with the splitter wedges and slippers produces a positive lift force. Thus, the comparison in Fig. 23 shows that the splitter wedges and slippers generate a disturbance that significantly increases the sled lift force. The correlation seems to provide a fairly useful method of accounting for the free-stream Mach number and sled height effects on the sled normal-force coefficient.
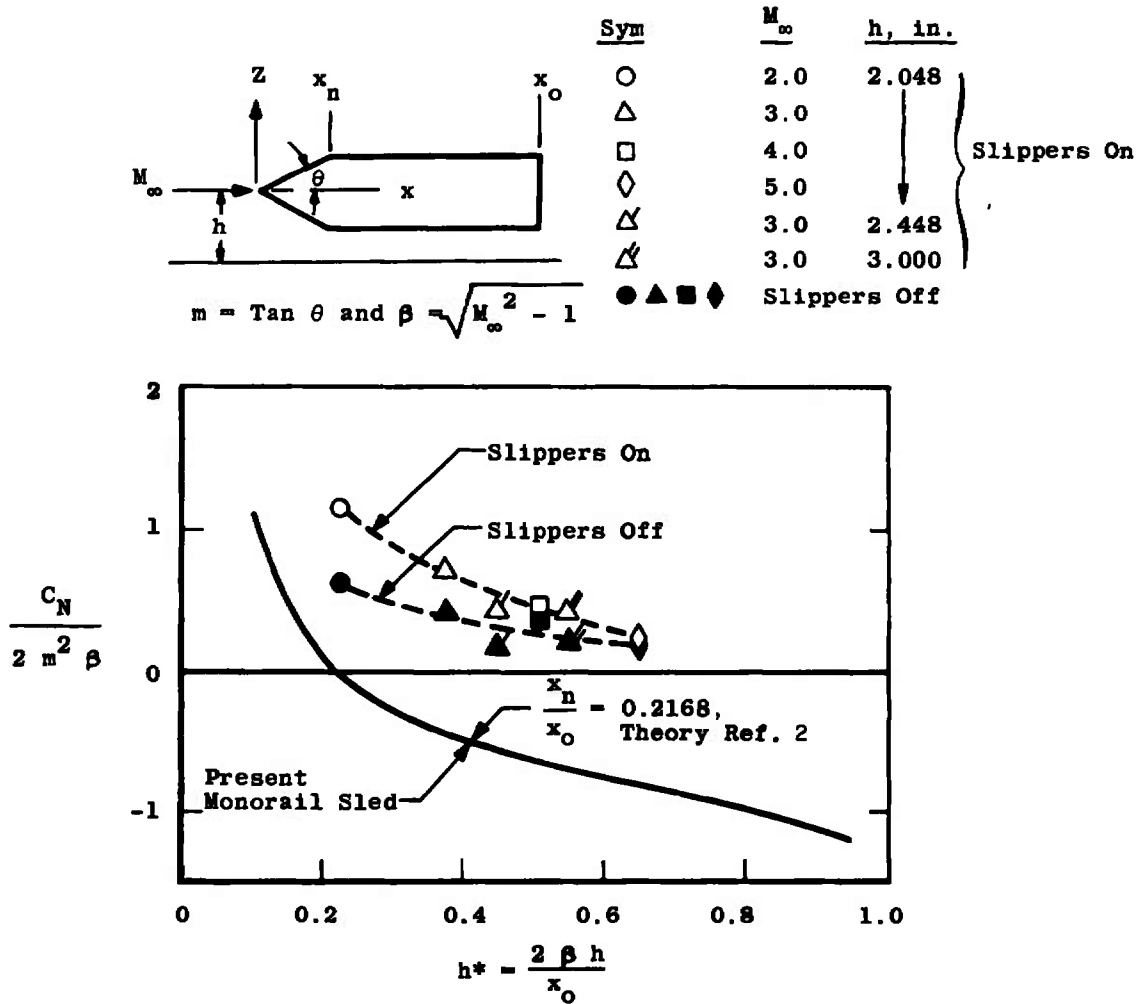
**Fig. 23 Comparison of Experiment and Theory for the Cone-Nose Sled
in Proximity to a Ground Surface**

SECTION IV
CONCLUDING REMARKS

These observations are based on wind tunnel results and are made
in the absence of a direct comparison with the full-scale track data.
Most of the wind tunnel data were obtained at Mach numbers 2, 3, 4,
and 5 at Reynolds numbers from 1.5 to 1.9 million. The wind tunnel
model was a 40-percent-scale version of the full-scale track vehicle,
but the slipper gap between the slipper and rail of the wind tunnel model
was equal to the full-scale slipper gap (that is, the wind tunnel model
slipper gap in terms of model scaling is 2.5 times too large). All other

wind tunnel model components, including the monorail cross-section, have been properly scaled to agree with the full-scale sled vehicle and track.

In the past, wind tunnel monorail sled data were obtained in the absence of sled slippers and without regard for the cross-sectional shape of the rail. The present tests, which were conducted with and without slippers attached to the sled, revealed that the slippers have a significant effect on the sled aerodynamic drag, normal force, and pitching moment.

Experimentally and theoretically, the aerodynamic normal-force coefficient of the sled configurations decreases with an increase in the height of the sled body above the rail surface or an increase in the free-stream Mach number. A comparison of the theoretical estimates and the experimental values of the sled normal force indicates that the presence of the sled splitter wedges and slippers produced a significant increase in the sled normal force at all free-stream Mach numbers from 2.0 to 5.0.

A comparison of the estimated full-scale aerodynamic loads on the cone- and spike-nose sled configurations shows that at Mach number 5.0, the normal force and forebody drag force of the two sled configurations differ by less than 3 percent. At Mach number 2.0, and in comparison to the cone-nose sled, the loading on the forward slipper of the spike-nose sled was nearly 30 percent smaller, and the forebody drag was almost 30 percent larger.

The aerodynamic drag attributed to the sled slippers appears to be independent of whether the sled nose is a 15-deg cone or a spike. This increment of slipper drag at Mach number 3.0 was also independent of the height of the sled body above the rail surface.

The wind tunnel models were tested with boundary-layer trips attached to the model surface. The trips produced turbulent boundary-layer flow over the wind tunnel model surface and, therefore, provided a better simulation of the turbulent boundary-layer characteristics on the full-scale vehicle. The wind tunnel results, when extrapolated to the full-scale Reynolds number at Mach number 3.0, indicate that the full-scale sled drag and slipper loading coefficients would be 3 or 4 percent below the wind tunnel values.

Preliminary estimates of the influence of the full-scale sled base drag on the slipper loads indicate that the base drag will theoretically increase the cone-nose sled slipper loads by 4 to 6 percent. For

example, this increase in slipper loading amounts to 37 lbf at Mach number 2 and 810 lbf at Mach number 5.0.

A small variation in the angle of roll (less than 6 deg) of the sled seemed to have little effect on the sled drag, normal force, and pitching moment. Rolling the sled vehicle produced a small unstable aerodynamic rolling moment.

The following recommendations are offered as possible means of improving the wind tunnel simulation of the full-scale track environment.

1. The influence of the wind tunnel model-slipper gap scaling on the aerodynamic coefficients is still questionable. Therefore, additional wind tunnel tests with a smaller model slipper gap would be useful in interpreting wind tunnel data.

2. The effectiveness of the air brakes located along the cylindrical body of the sled could be evaluated in a wind tunnel test program.

3. If a significant unresolved disagreement still exists between the full-scale and wind tunnel test results, then an attempt could be made to improve the wind tunnel simulation of the full-scale flow field environment by removing the boundary layer forming on the rail upstream of the sled model by suction.
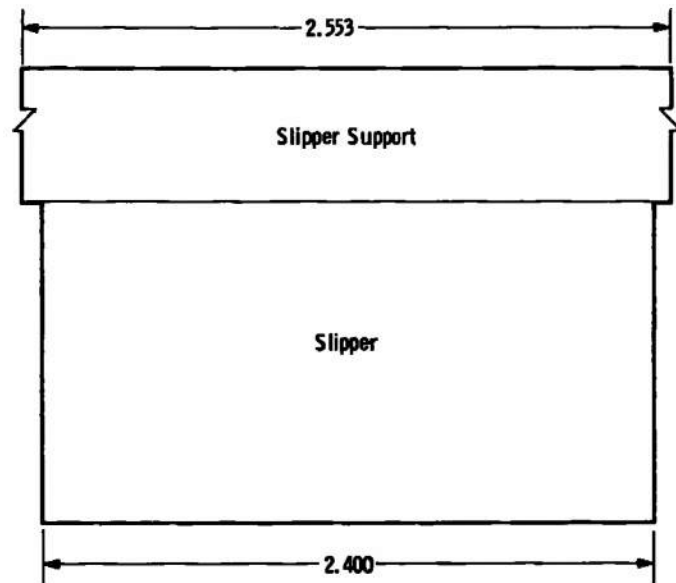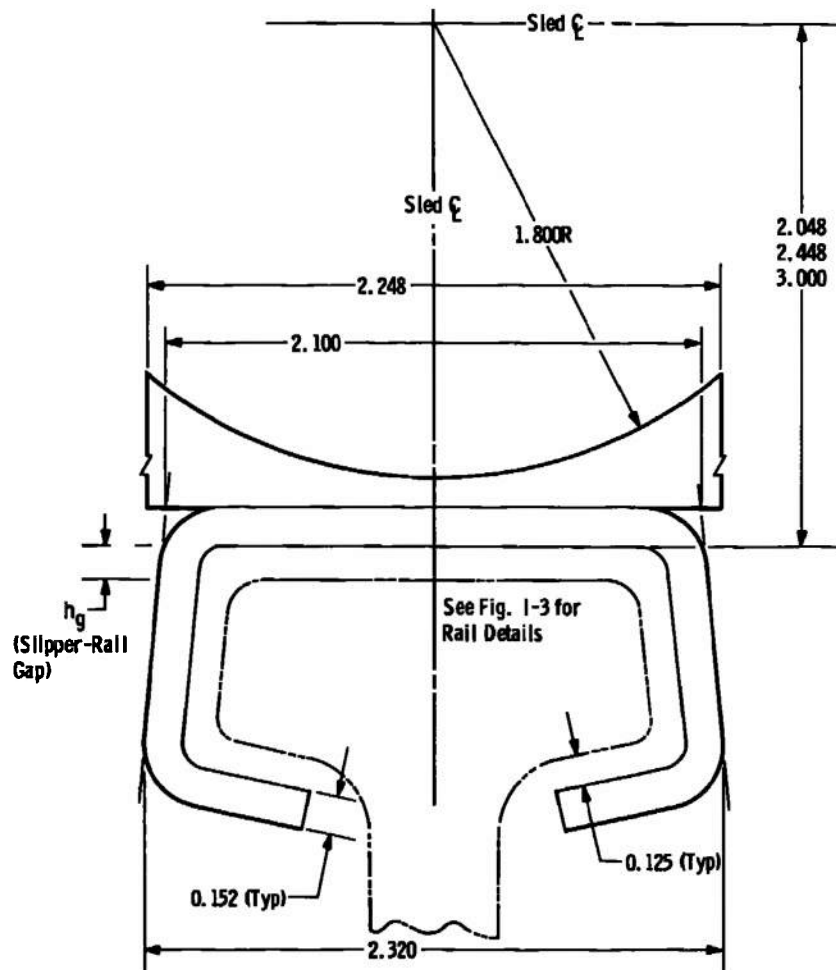
The present wind tunnel results indicate that the forward slipper loads at Mach number 5 on the full-scale vehicle approach 2700 lbf. A wind tunnel test program could be used to define model configurations that would reduce these slipper loads.

REFERENCES

1. Krupovage, D. J., Mixon, L. C. and Pokorny, O. T., Capt. "Wind Tunnel and Full-Scale Forces on Rocket Sleds." AFMDC-TR-67-12, January 1967.

2. Hermann, R., Moynihan, F. and Melnik, W. "Aerodynamic Investigation of Sled Configurations for the Holloman Track." AFMDC-TR-59-18 (AD232463), June 1959.

3. Lubliner, J., Oliver, R. E., and Morgan, A. J. A. "Low-to-High-Speed Drag Compilations for Rocket Test Sled Components." NAVORD Report 5635, August 1957.
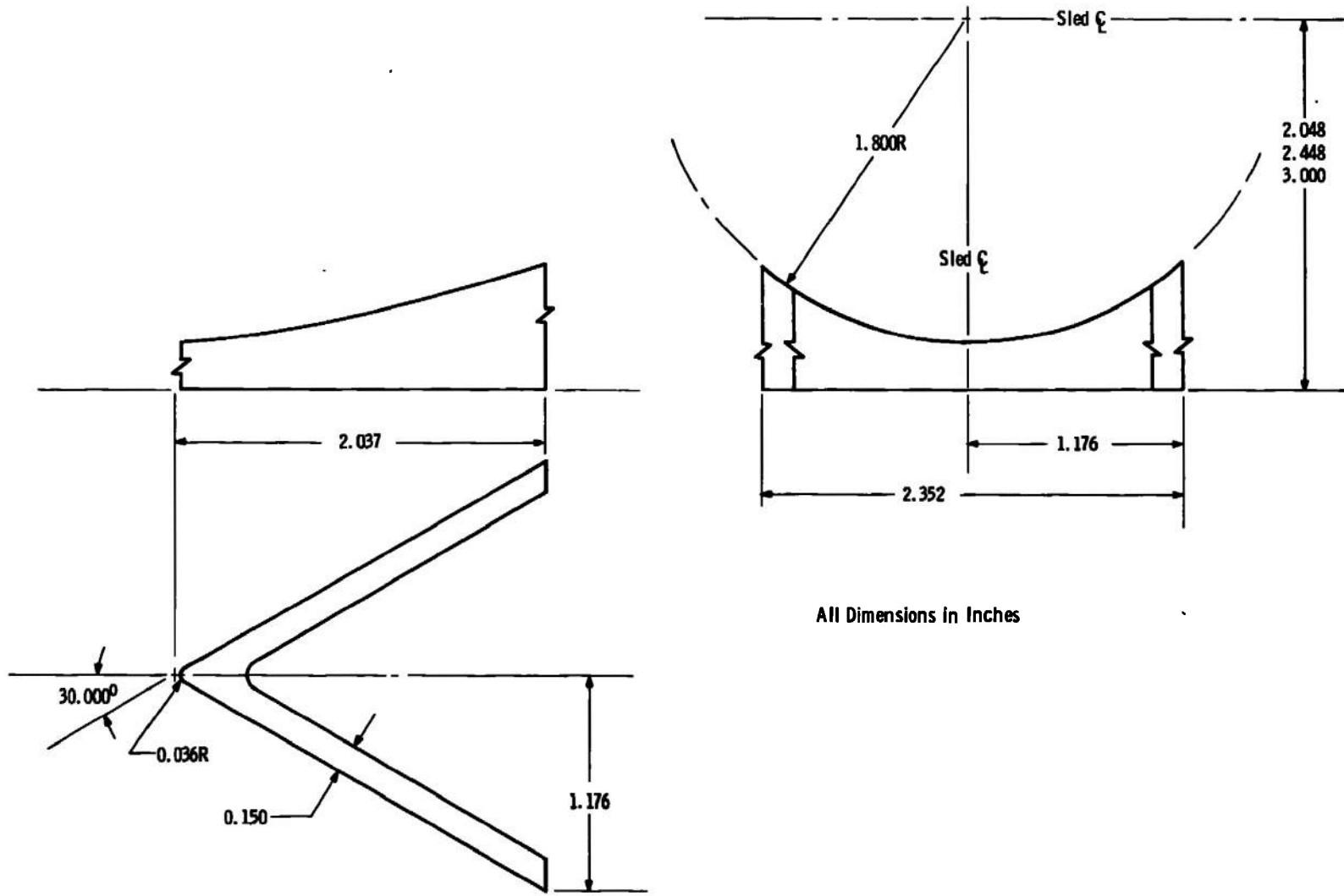
APPENDIXES
I. MODEL CONFIGURATION DETAILS
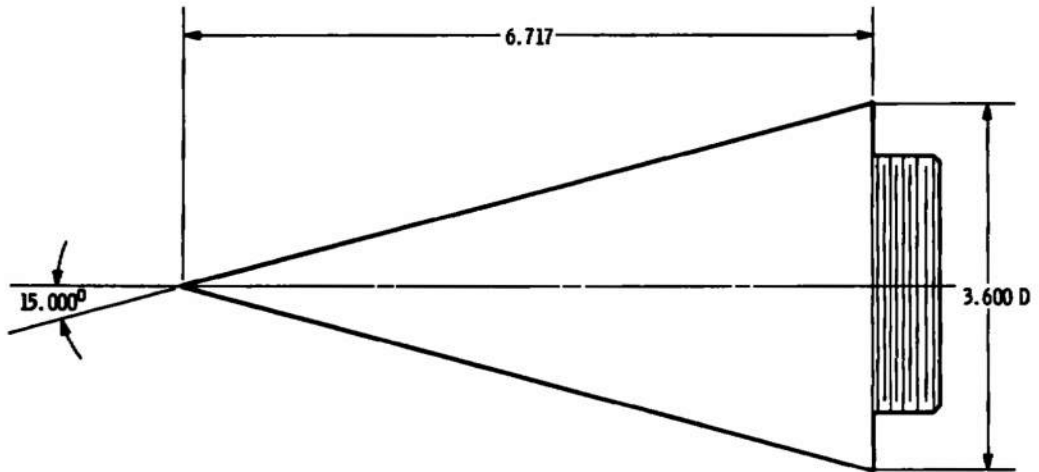II. DATA REDUCTION PROCEDURES AND NOMENCLATURE
III. BASIC SLED POSITIONING DATA

Fig. I-1 Slipper Details

1.800R

Sled ₵

Sled ₵

2.048
2.448
3.000

1.176

2.352
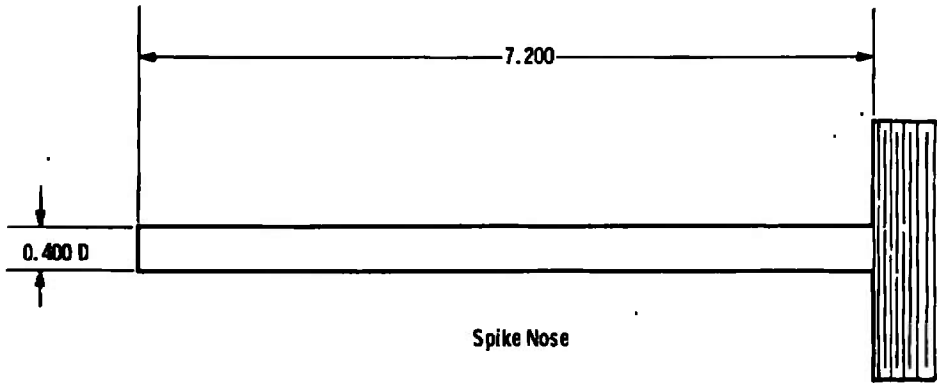
2.037

30.000°

0.036R

0.150

1.176

All Dimensions in Inches

Fig. I-2 Splitter Wedge Details

Cone Nose

Spike Nose

All Dimensions in Inches
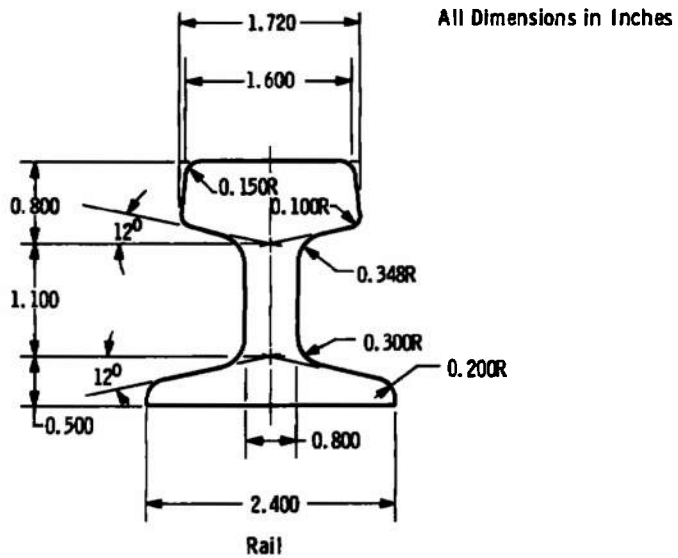
Rail

Fig. I-3 Nose and Rail Details
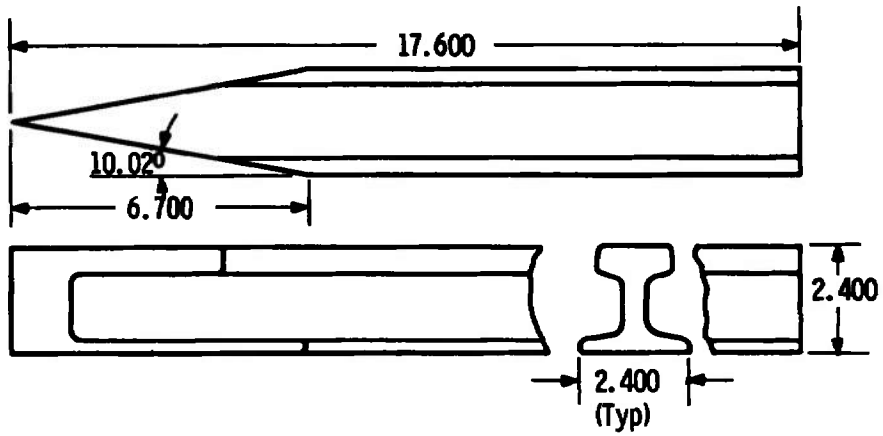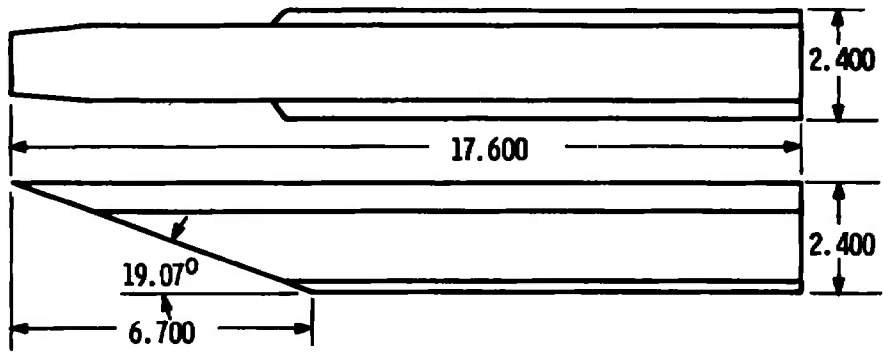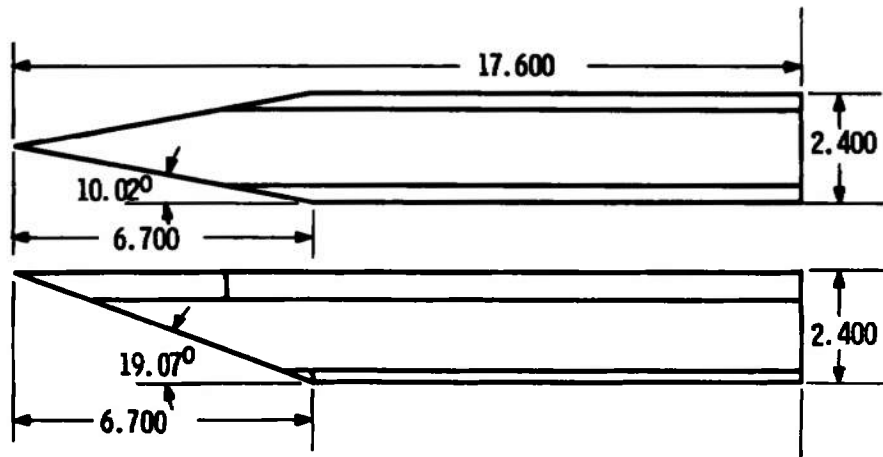
Fig. I-4 Rail Tip Configurations

APPENDIX II
DATA REDUCTION PROCEDURES AND NOMENCLATURE

The wind tunnel test results were evaluated in such a manner as to facilitate the use of these data in estimating the performance of the full-scale sled. Therefore, these wind tunnel results are not only presented in terms of the conventional aerodynamic coefficients, but also in terms of the loads imposed on the sled slippers which guide the sled along the track. The orientation of the aerodynamic loads and the coordinate system used in the wind tunnel tests is shown in Fig. II-1a. The corresponding coordinate system employed at the Holloman Air Force Base track facility is shown in Fig. II-1b and differs slightly from the wind tunnel coordinates. These differences in coordinate systems will result in a difference in the sign of the sled side force as shown listed in Fig. II-1b.
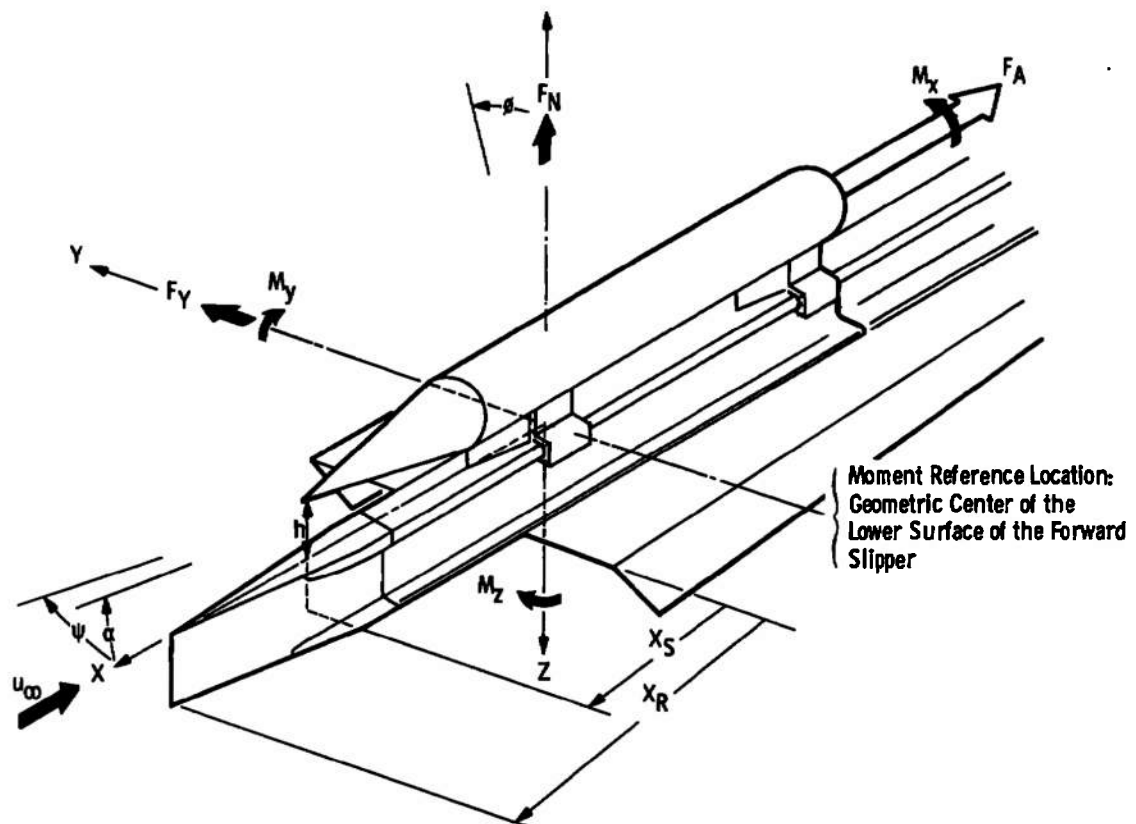
a. Wind Tunnel Coordinate System

Fig. II-1 Comparison of Wind Tunnel and Full-Scale Track Coordinate System
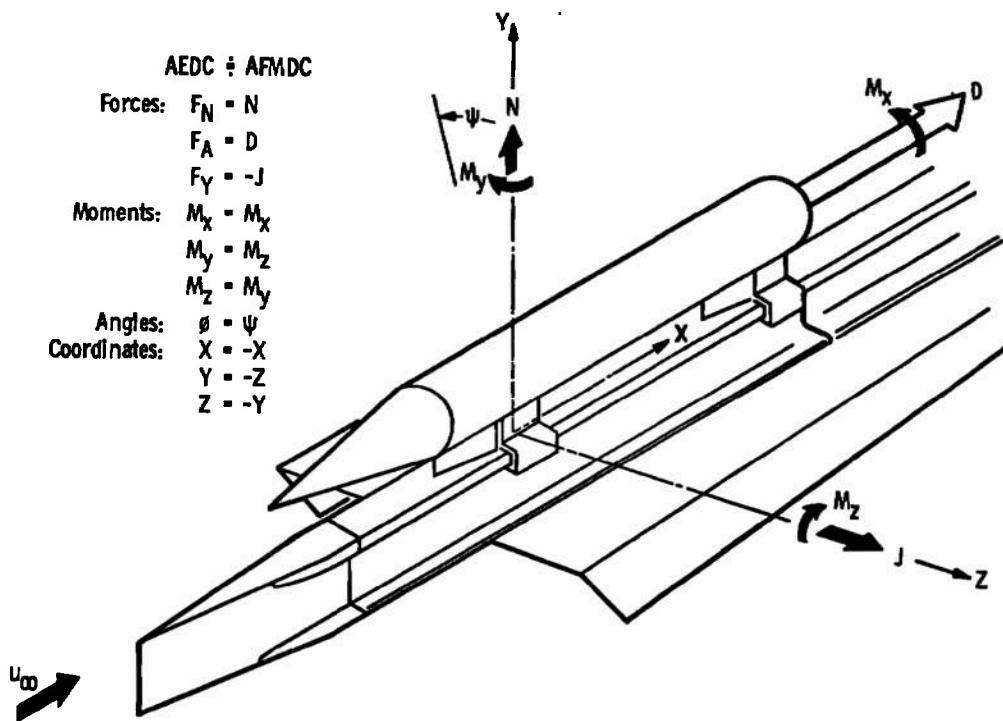
b. Track Coordinates System

Fig. II-1 Concluded

In this analysis, the sled aerodynamic loads as experienced by the slipper are defined as positive coefficients or slipper loadings if the load tends to move the sled away from the rail. Conversely, a negative coefficient or slipper loading will indicate a force that tends to move the sled toward the rail.

The aerodynamic loading imposed on the wind tunnel model was recorded by means of a strain-gage balance having an axis that coincided with the model axis. This balance measures the moments about a particular balance reference point lying along the balance axis and also the forces imposed on the model; that is, the normal force (F_N) axial force (F_A), and side force (F_Y). The location of these forces in terms of the center of loading or the point where the moment resulting from any one of these forces is zero is not explicitly defined, but the measured moments in the pitch, yaw, and roll planes (that is, M_y, M_z, and M_x) are used to locate the resultant force vectors in these three planes. The measured forces define the magnitude and orientation of the resultant force vector, and the moments determine the displacement of this resultant vector from any given point on the sled model.

The common reference point for moments in the pitch and yaw planes of the sled was selected as the center of the lower surface of the forward monorail slipper (Fig. II-2). These moments, which were recorded at the balance moment reference center were transferred to the forward slipper reference point. A synopsis of the analysis used in defining the forces and moment in each of the three planes of the sled is presented in the following discussion:

Pitch Plane of the Sled

The following figure describes the basic nomenclature and approach used in defining the loading on the sled as defined by the forces and moments in the pitch plane of the sled.
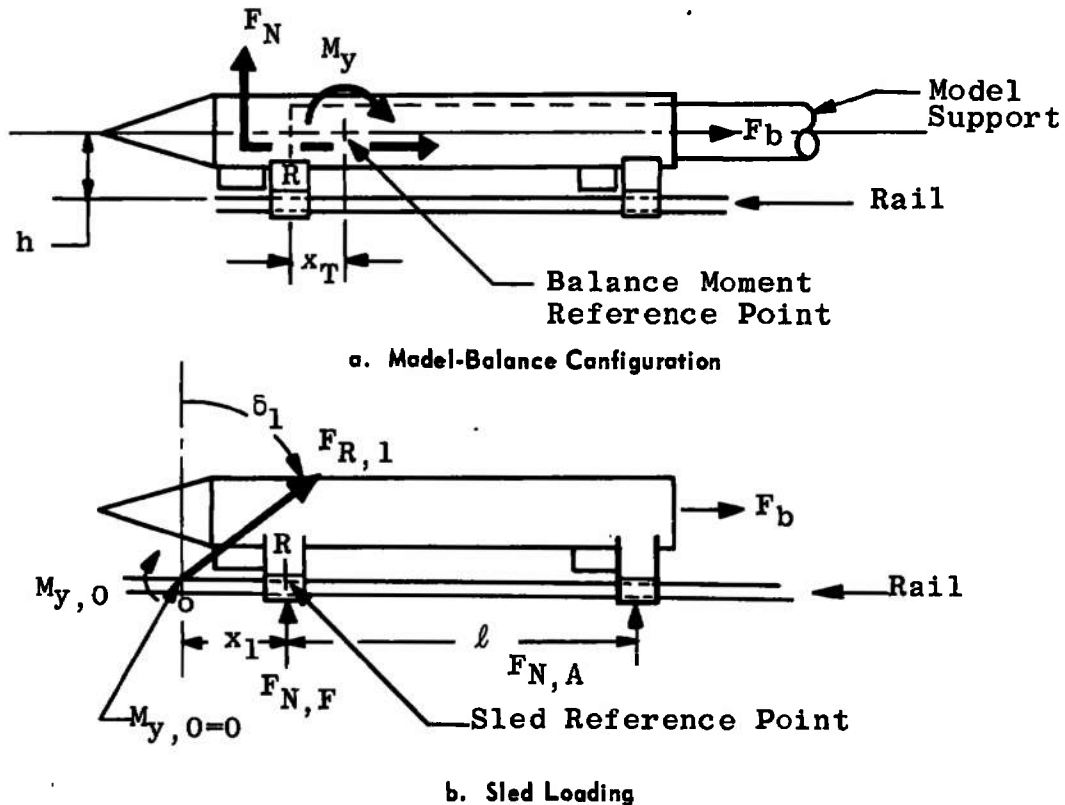

a. Model-Balance Configuration

b. Sled Loading

Fig. II-2 Pitch Plane of the Sled

The resultant pitching moment (that is, the moment attributed to F_N and F_A) about the forward slipper model reference point (R) is simply

$$M_{y,R} = (x_1 \cos \delta_1) F_{R,1} \quad \text{or}$$
$$= F_N (x_1)$$

(II-1)

The angular orientation and location of the resultant force vector $F_{R,1}$ is defined as

$$\delta_1 = \tan^{-1}\left[(F_{A,T} - F_b)/F_N\right] \tag{II-2}$$

The parameter F_b is the wind tunnel model base drag, and $F_{A,T}$ is the drag force as recorded by the balance. The difference $(F_{A,T} - F_b)$ represents the forebody drag of the sled and is denoted as F_A. The term $F_{R,1}$ is the resultant force vector which is defined as

$$F_{R,1} = \sqrt{F_N^2 + F_A^2} \tag{II-3}$$

The location of $F_{R,1}$, relative to R, is obtained in the following manner from Fig. II-1a.

$$M_{y,R} = M_y + F_{R,1}(h \tan \delta_1 - x_T)\cos \delta_1 \tag{II-4}$$

Combining the expressions from Eqs. (II-1) and (II-4) yields the following expression for x_1.

$$x_1 = M_y/(F_{R,1} \cos \delta_1) + h \tan \delta_1 - x_T$$

or

$$x_1 = (M_y/F_N) + h \tan \delta_1 - x_T \tag{II-5}$$

This evaluation does not require that any assumption be made concerning the actual location of the line of action of the axial-force component, $F_{A,T}$. Obviously, the magnitudes of $F_{R,1}$, δ_1, and x_1 are dependent on the base pressure loading, F_b.

The aerodynamic sled loading imposed on the forward and aft slipper support, namely $F_{N,F}$ and $F_{N,A}$, are as follows:

$$F_{N,F} = F_{R,1}\left[\cos \delta_1 + (\ell_1/\ell)\right] \tag{II-6}$$

where

$$\ell_1 = ((M_y/F_N) - x_T + h \tan \delta_1)\cos \delta_1$$

$$F_{N,A} = -F_{R,1}(\ell_1/\ell) \tag{II-7}$$

Yaw Plane of the Sled

The nomenclature used in defining the loading on the sled in the yaw plane is shown in the following figure.
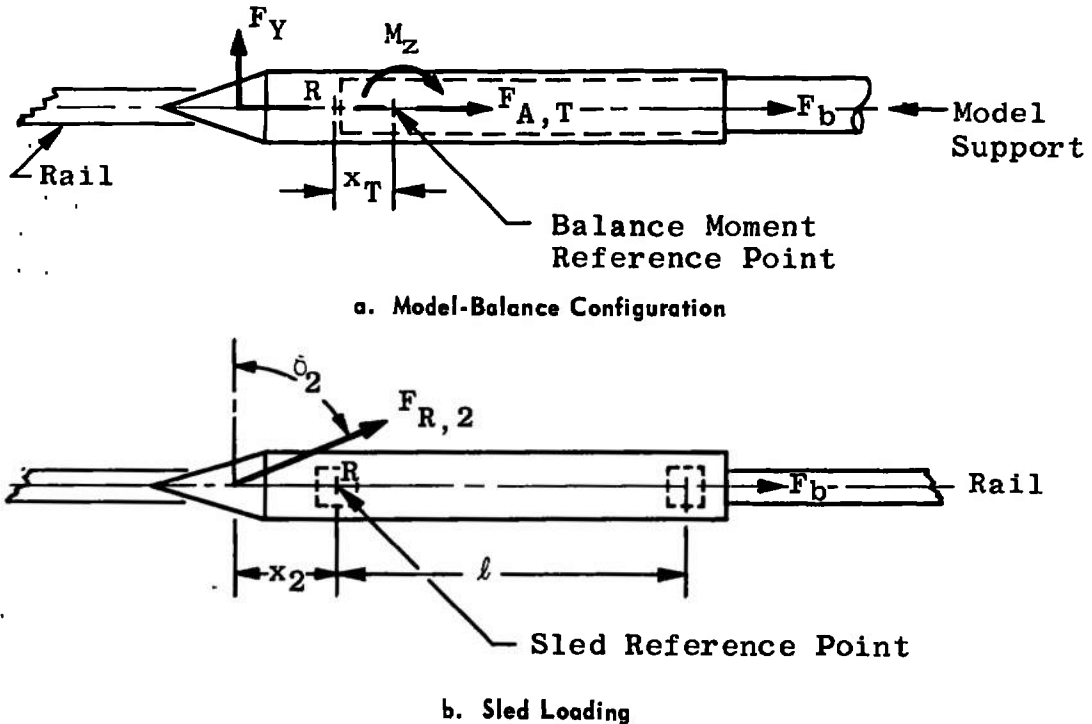
a. Model-Balance Configuration

b. Sled Loading

Fig. II-3 Yaw Plane of the Sled (Top View)

The resultant yawing moment about the forward slipper model reference point (R) is simply

$$M_{z,R} = F_{R,2} (x_2 \cos \delta_2) \qquad (II-8)$$

or

$$= F_Y (x_2)$$

where

$$\delta_2 = \tan^{-1} (F_A/F_Y) \qquad (II-9)$$

and

$$F_{R,2} = \sqrt{F_A^2 + F_Y^2} \qquad (II-10)$$

The location of the resultant force vector, $F_{R,2}$, is obtained in the following manner.

$$M_{z,R} = M_z + F_{R,2}(x_T \cos \delta_2) \qquad (II-11)$$

The location, x_2, of the resultant force vector ($F_{R,2}$) was obtained by combining Eqs. (II-8) and (II-11).

$$x_2 = M_z/(F_{R,2} \cos \delta_2) - x_T$$

$$= M_z/F_Y) - x_T \qquad (II-12)$$

Roll Plane of the Sled

Two reference points (R and Q in Fig. II-4) were used in defining the loading imposed on the sled vehicle in the roll plane. The first reference point was designated as the center of the slipper (R), and the second was selected as the point of contact between the slipper and the rail surface (that is, at point Q in Fig. II-4).
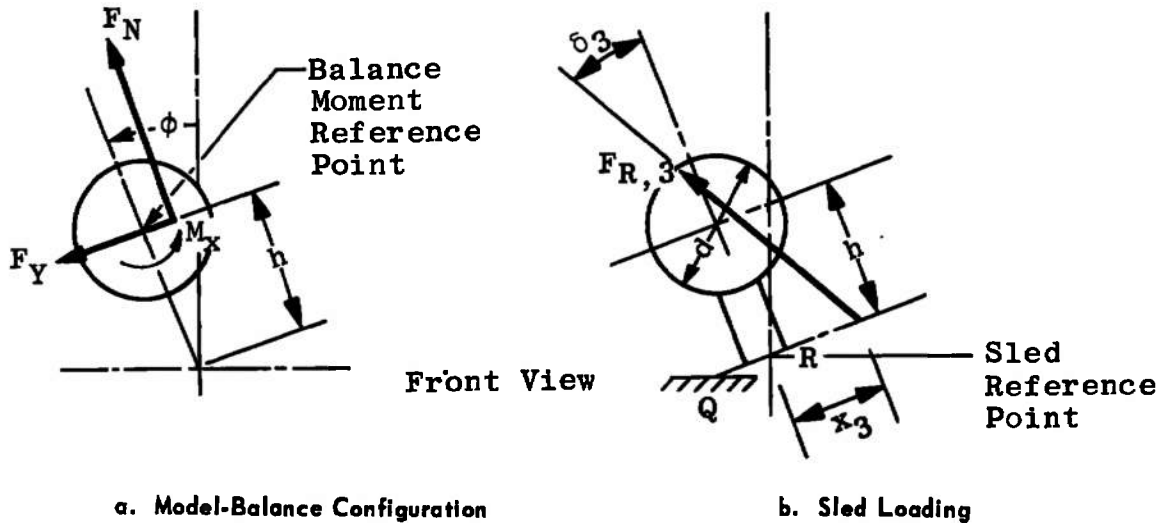

a. **Model-Balance Configuration**   b. **Sled Loading**

Fig. II-4 Roll Plane of the Sled

The resultant rolling moment about point R is defined as

$$M_{x,R} = F_{R,3} \, (x_3 \cos \delta_3) \tag{II-13}$$

or

$$= F_N \, (x_3)$$

where

$$\delta_3 = \tan^{-1}(F_Y/F_N) \tag{II-14}$$

$$F_{R,3} = \sqrt{F_N^2 + F_Y^2} \tag{II-15}$$

The location of the resultant force vector from the moment reference point, R, along the lower surface of the slipper in the roll plane is obtained in the following manner.

$$M_{x,R} = M_x + F_{R,3} \, (h \sin \delta_3) \tag{II-16}$$

Using Eqs. (II-13) and (II-16), the following expression for x_3 was obtained

$$x_3 = M_x/(F_{R,3} \cos \delta_3) + h \tan \delta_3 \tag{II-17}$$

$$= (M_x/F_N) + h \tan \delta_3$$

50

The moment about point "Q," the contact point between the slipper and the rail, varies with the angle of roll. For example, at a roll angle of zero, the rolling moment for this symmetrical configuration should be zero; and for finite angles of roll, the contact point is located nominally at the outer edge of the rail. In the case of the wind tunnel model, this length from point Q to R (that is, $\overline{QR}$) is about 0.80 in. Thus, the moment about "Q" when the roll angle is positive is as follows:
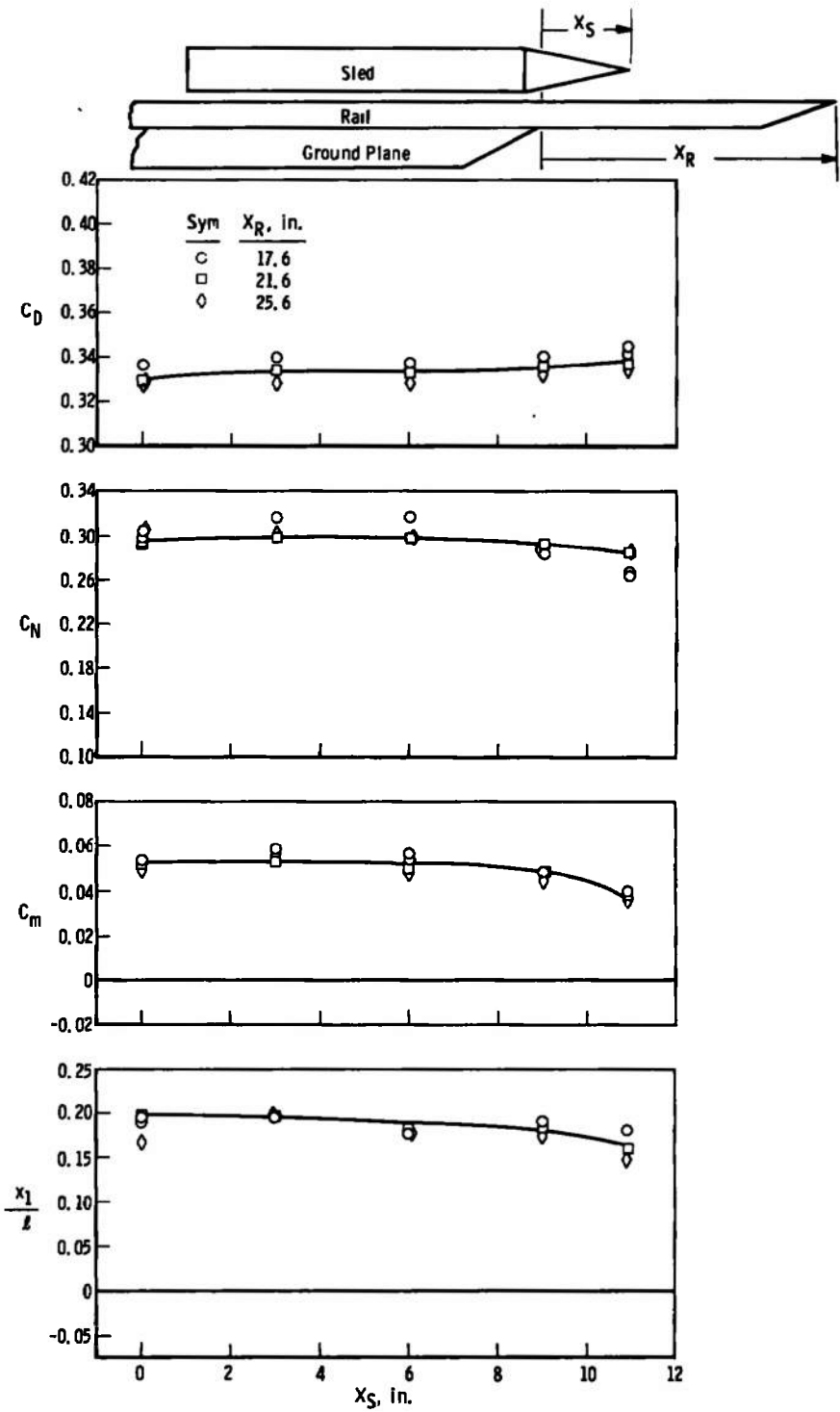
$$M_{x,Q} = F_{R,3}(0.80 + x_3)\cos\delta_3; \text{ for } \phi > 0$$
$$= F_N(0.80 + x_3)$$
$$M_{x,Q} = \pm\, 0.80\, F_N; \text{ for } \phi = 0 \qquad (II\text{-}18)$$
$$M_{x,Q} = -\,F_N(0.80 + x_3); \text{ for } \phi < 0$$

The evaluation of this moment $(M_{x,Q})$ when added to the moment produced by the weight and motion of the sled will be used to determine the roll stability of the sled as it moves along the track.
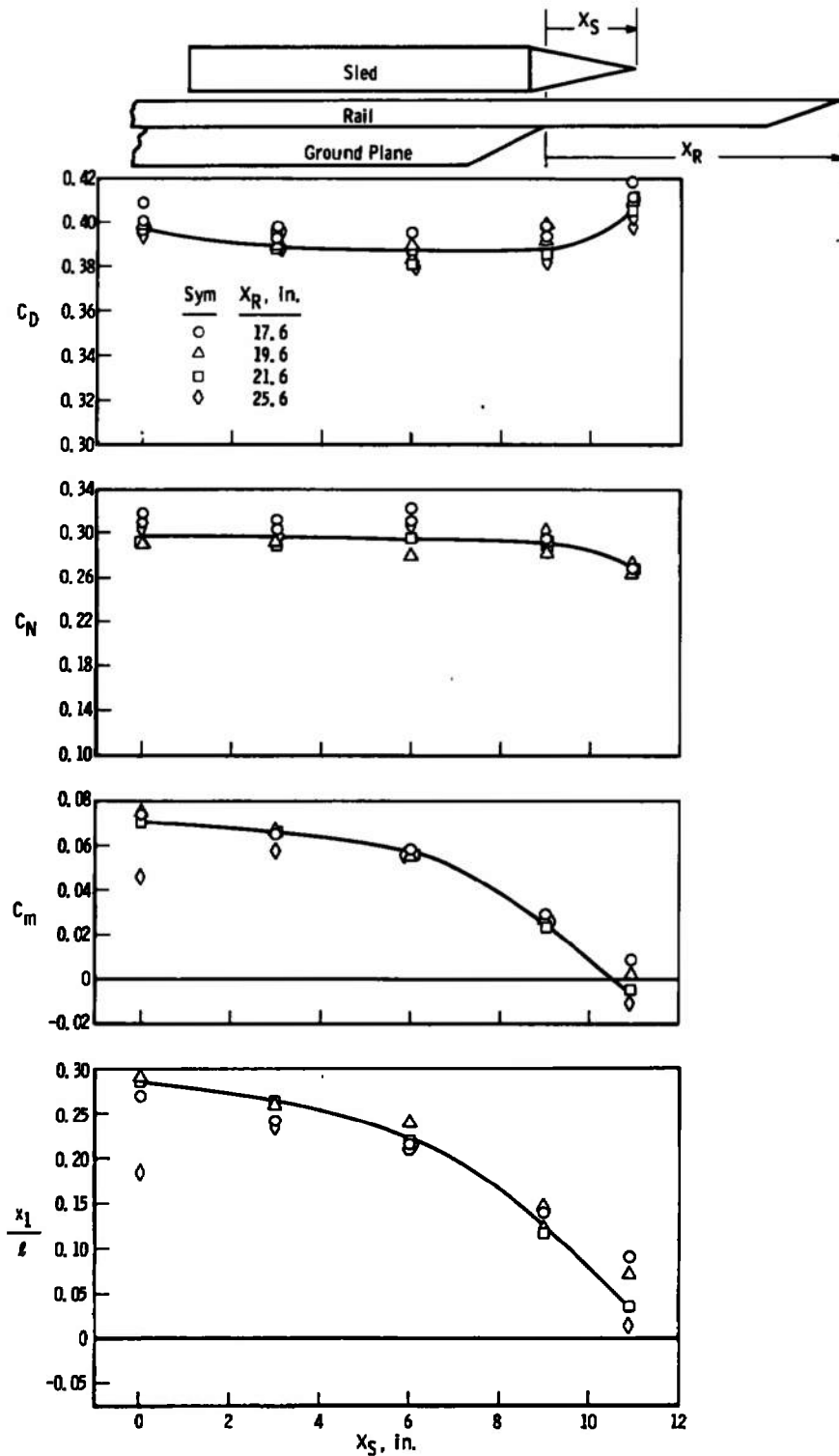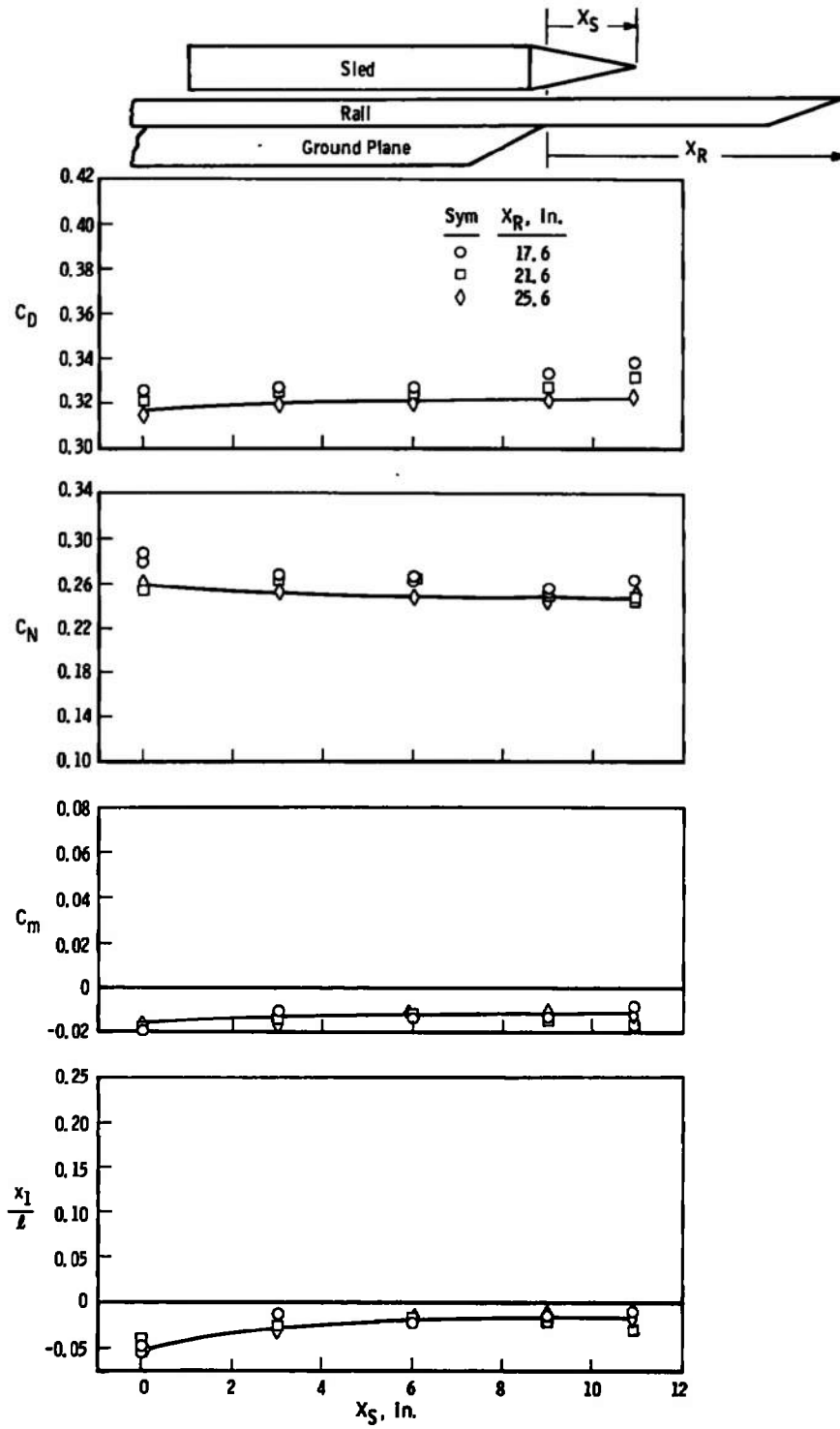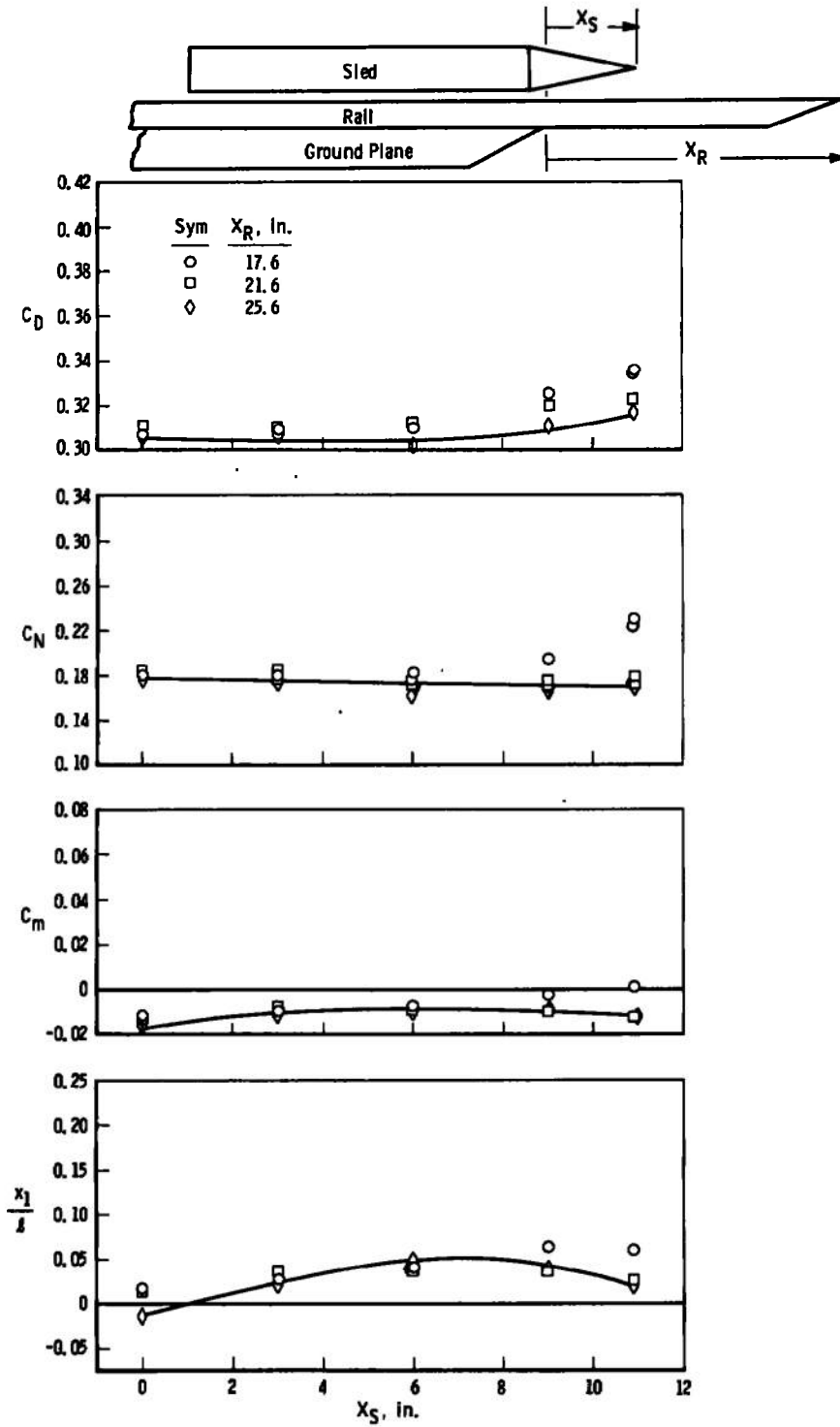
a. $M_\infty = 2.0$; $Re_d = 1.5 \times 10^6$

Fig. III-1 Effect of Sled and Rail Locations on the Aerodynamic Sled Loadings

b. $M_{\infty} = 3.0$; $Re_d = 1.8 \times 10^6$

Fig. III-1 Continued

c. $M_\infty = 4.0$, $Re_d = 1.8 \times 10^6$

Fig. III-1 Continued

d. $M_\infty = 5.0$; $Re_d = 1.9 \times 10^6$
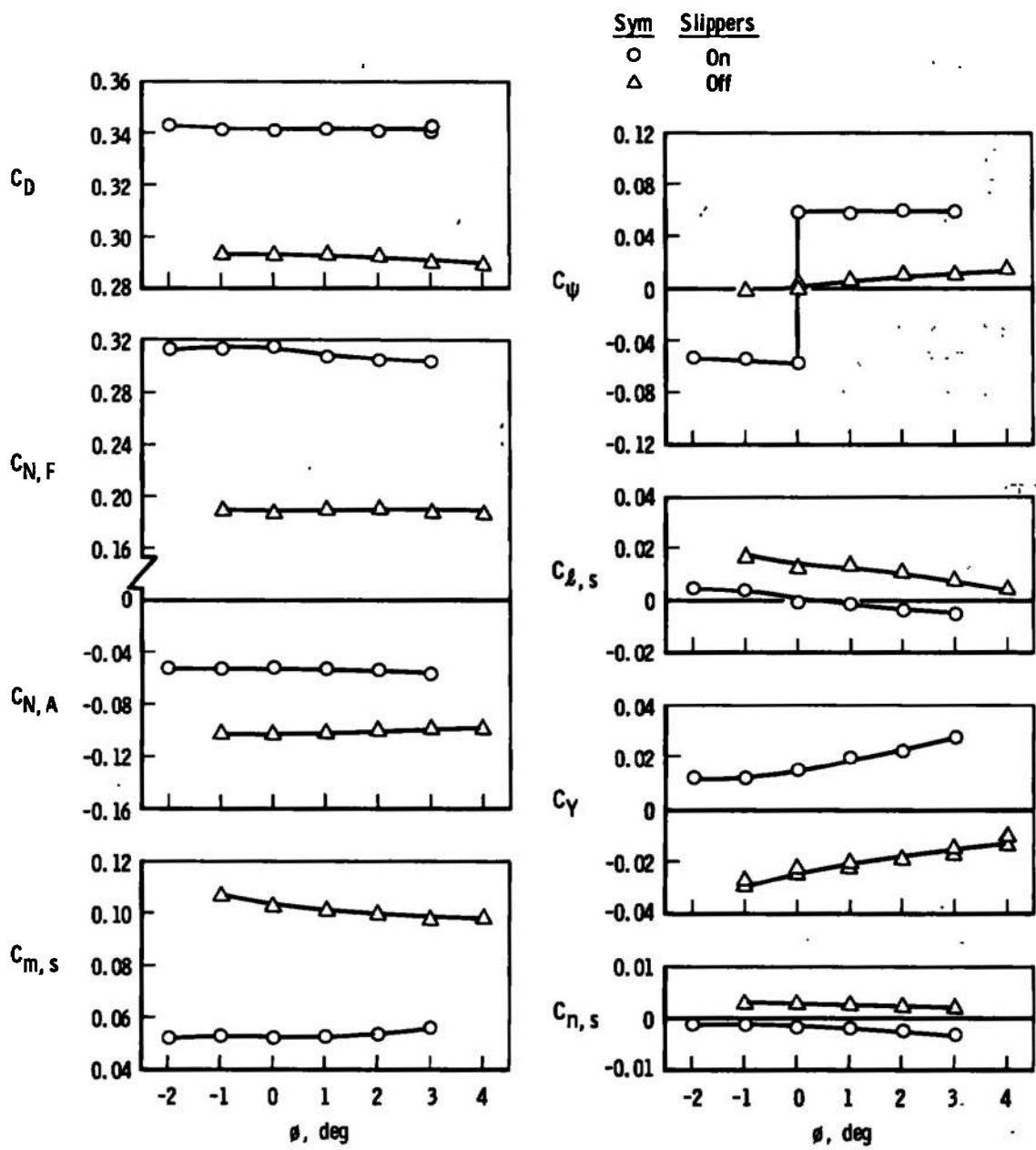
Fig. III-1 Concluded

Fig. III-2 Effect of Roll Angle on Sled Loading, $M_\infty = 3.0$ and $Re_d = 1.8 \times 10^6$

DOCUMENT CONTROL DATA - R & D

(Security classification of title, body of abstract and indexing annotation must be entered when the overall report is classified)

1 ORIGINATING ACTIVITY *(Corporate author)*	2a. REPORT SECURITY CLASSIFICATION
Arnold Engineering Development Center ARO, Inc., Operating Contractor Arnold Air Force Station, Tenn. 37389	UNCLASSIFIED
	2b. GROUP N/A

3 REPORT TITLE

EVALUATION OF WIND TUNNEL TESTS ON AFMDC MONORAIL CONE- AND SPIKE-NOSE SLED CONFIGURATIONS AT MACH NUMBERS FROM 2.0 TO 5.0

4 DESCRIPTIVE NOTES *(Type of report and inclusive dates)*
Final Report   February 27 to April 23, 1968

5 AUTHOR(S) *(First name, middle initial, last name)*
W. T. Strike, Jr., and E. J. Lucas, ARO, Inc.

6 REPORT DATE	7a. TOTAL NO. OF PAGES	7b. NO. OF REFS
December 1968	66	3

8a. CONTRACT OR GRANT NO.	9a. ORIGINATOR'S REPORT NUMBER(S)
F40600-69-C-0001	AEDC-TR-68-198
b. PROJECT NO 6876	
c. Program Element 6540215F	9b. OTHER REPORT NO(S) *(Any other numbers that may be assigned this report)*
d	N/A

10 DISTRIBUTION STATEMENT This document has been approved for public release and sale; its distribution is unlimited.

11 SUPPLEMENTARY NOTES	12. SPONSORING MILITARY ACTIVITY
Available in DDC.	Air Force Missile Development Center (MDTT), Holloman AFB, New Mexico 88330

13 ABSTRACT

An evaluation was made of the results of wind tunnel tests on 0.4-scale models of two Holloman Air Force Base monorail rocket-sled configurations. The sled models consisted of a cylindrical body with forward and aft splitter wedges and slippers and with an interchangeable 15-deg cone nose and spike nose. The wind tunnel tests were conducted at Mach numbers 2, 3, 4, and 5 and over a Reynolds number range (based on the sled body diameter) from 0.22 to 1.92 million. The sled model was sting supported over a scaled replica of the Holloman track rail which was supported on a sharp-leading-edge ground plane (flat plate). The test results consist of static force measurements obtained from a six-component strain-gage balance. Also, pitot pressure flow field surveys were made over the ground plane and model rail in the region occupied by the sled model. The following model parameters were varied during the test: the location of the sled relative to the rail tip and also to the ground plane leading edge, the height of the sled body above the rail surface, the gap between the slipper and rail surface, and the sled roll angle. The results presented include an evaluation of the influence of the sled slippers, the free-stream Reynolds number, and the Mach number on the aerodynamic loading of the sled.

DD FORM 1 NOV 65 1473

14 KEY WORDS	LINK A		LINK B		LINK C	
	ROLE	WT	ROLE	WT	ROLE	WT
wind tunnel tests						
rocket sleds						
configuration effects						
supersonic flow						
aerodynamic loads						